Theories of Multiple Equilibria and Weather Regimes—A Critical Reexamination. Part II: Baroclinic Two-Layer Models

PRISCILLA CEHELSKY AND KA KIT TUNG*

Department of Mathematics, Massachusetts Institute of Technology, Cambridge, MA 02139

(Manuscript received 13 October 1986, in final form 1 June 1987)

ABSTRACT

Previous results based on low- and intermediate-order truncations of the two-layer model suggest the existence of multiple equilibria and/or multiple weather regimes for the extratropical large-scale flow. The importance of the transient waves in the synoptic scales in organizing the large-scale flow and in the maintenance of weather regimes was emphasized. Our result shows that multiple equilibria/weather regimes that are present in lower order models examined disappear when a sufficient number of modes are kept in the spectral expansion of the solution to the governing partial differential equations. Much of the chaotic behavior of the large-scale flow that is present in intermediate order models is now found to be spurious. Physical reasons for the drastic modification are offered.

We further note a peculiarity in the formulation of most existing two-layer models that also tends to exaggerate the importance of baroclinic processes and increase the degree of unpredictability of the large-scale flow.

1. Introduction

It is known that the zonal flow of the atmosphere in the extratropics is unstable baroclinically to synoptic-scale perturbations. On the planetary scale, asymmetric perturbations are dominated by quasi-stationary waves forced mainly by flow over continental elevations and by differential heating. The nonlinear interactions of the synoptic and planetary scales of the flow in the extratropics form the subject of study in the present paper. In particular, we are interested in the effect of the transient synoptic waves on the low-frequency variability of the planetary-scale waves.

The life cycles of the unstable baroclinic disturbances produce natural and perhaps unpredictable variability in the synoptic scales. Through nonlinear interactions, some variability in the large-scale flow is inevitably induced. What is not clear at this point is the *degree* to which the large-scale flow is affected. An understanding of this issue is crucial in any study of the long-range predictability of the large-scale flows in the atmosphere.

Implicit in the work of Charney and DeVore (1979) and Charney and Straus (1980, hereafter referred to as CS) is the hypothesis that the synoptic-scale "instabilities" serve to initiate transitions in the atmospheric large-scale flow from one persistent "equilibrium" state to another. These large-scale persistent flow regimes are largely determined and maintained by the nonlinear interactions of the large-scale wave-mean flow system itself. An almost opposite point of view is developed in the work of Reinhold and Pierrehumbert (1982, hereafter referred to as RP; see also the corrigendum to that paper, Reinhold and Pierrehumbert, 1985). They suggest that the transient synoptic-scale waves are of primary importance not only in initiating transitions from one persistent flow regime to another, but are also responsible for organizing and maintaining the large-scale regimes themselves. It is interesting to note that the two different conclusions are inferred from the same set of governing partial differential equations and differ only in the degree of approximation (i.e., level of truncation) used to obtain the respective solutions. Similar to the conclusions drawn in Part I for the barotropic models, we will show (in section 3) that the solution of RP cannot be treated as a better approximation to the original partial differential equations than that of CS even though the truncation used by RP is less severe. We will show and explain why intermediate truncation levels may in most instances yield misleading results behaving very differently from the true solution. In particular, we will show that the converged solution is found to have only one "weather regime" for the large-scale flow where, previously, multiple regimes were found in lower order models. Our result cannot, however, be taken as a "proof" that multiple weather regimes do not exist.

2. The two-layer model

The two-layer model used in this study is a general extension of the low- and intermediate-order models of CS and RP. Our formulation allows an arbitrary number of terms to be kept in the spectral expansion of the model equations (within the limits of computational space and time). Thus full nonlinearity can be retained. The present model supports nonlinear inter-

* Present Affiliation: Department of Mathematics and Computer Science, Clarkson University, Potsdam, NY 13676.

actions among the planetary-, synoptic- and small-scale waves. In this section we review the development of the two-layer model and introduce a more general notation. The original formulation is due to Lorenz (1960, 1963).

Consider a midlatitude, periodic β-plane channel centered at latitude φ_0. The meridional boundaries of the channel are at $y = 0$ and πL. The characteristic depth of each layer is H. The governing quasi-geostrophic vorticity, thermodynamic energy and thermal wind equations are

$$\frac{\partial}{\partial t}\nabla^2\psi = -J(\psi, \nabla^2\psi) - J(\tau, \nabla^2\tau) - \beta_0\frac{\partial\psi}{\partial x} - \frac{1}{2}J\left(\psi - \tau, \frac{f_0 h}{H}\right) - \frac{1}{2}k_d\nabla^2(\psi - \tau) \tag{2.1}$$

$$\frac{\partial}{\partial t}\nabla^2\tau = -J(\psi, \nabla^2\tau) - J(\tau, \nabla^2\psi) - \beta_0\frac{\partial\tau}{\partial x} - \frac{f_0 w}{H} - 2k'_d\nabla^2\tau + \frac{1}{2}k_d\nabla^2(\psi - \tau) + \frac{1}{2}J\left(\psi - \tau, \frac{f_0 h}{H}\right) \tag{2.2}$$

$$2\frac{\partial}{\partial t}\theta = -J(\psi, 2\theta) - \frac{\sigma}{H}w + 2h'_d(\theta^* - \theta) \tag{2.3}$$

$$\nabla^2\theta = A\nabla^2\tau, \tag{2.4}$$

which have been finite differenced in the vertical direction. The following notation has been used:

φ	latitude
φ_0	mid-channel reference latitude
a	radius of the earth
Ω	angular velocity of the earth
t	time
x	zonal coordinate
y	meridional coordinate ($dy = ad\varphi$)
f_0	($=2\Omega\sin\varphi_0$), Coriolis parameter at latitude φ_0
β_0	$[=(df/dy)\varphi_0]$, meridional gradient of the Coriolis parameter at latitude φ_0
∇^2	$[=(\partial^2/\partial x^2) + (\partial^2/\partial y^2)]$, horizontal Laplacian
$J(f, g)$	$\left[=\frac{\partial f}{\partial x}\frac{\partial g}{\partial y} - \frac{\partial f}{\partial y}\frac{\partial g}{\partial y}\right]$, horizontal Jacobian
$\psi_1(x, y, t)$	upper layer geostrophic streamfunction
$\psi_2(x, y, t)$	lower layer geostrophic streamfunction
$\psi(x, y, t)$	$[=\frac{1}{2}(\psi_1 + \psi_2)]$, mean streamfunction
$\tau(x, y, t)$	$[=\frac{1}{2}(\psi_1 - \psi_2)]$, shear streamfunction
$w(x, y, t)$	vertical velocity at the interface
$\theta_1(x, y, t)$	upper layer potential temperature
$\theta_2(x, y, t)$	lower layer potential temperature
$\theta(x, y, t)$	$[=\frac{1}{2}(\theta_1 + \theta_2)]$, mean potential temperature
$\theta^*(x, y)$	radiative equilibrium mean potential temperature
$h(x, y)$	topographic height
H	characteristic depth of each layer
σ	static stability parameter
k_d	Ekman damping coefficient at the bottom surface
k'_d	frictional coefficient at the interface
h'_d	Newtonian cooling coefficient
A	$\left\{=\frac{2f_0}{c_p}\left[\left(\frac{P_2}{P_{00}}\right)^\kappa - \left(\frac{P_1}{P_{00}}\right)^\kappa\right]\right\}$, where c_p is the specific heat at constant pressure, R is the universal gas constant and $\kappa = R/C_p$.
P_1	upper layer pressure
P_2	lower layer pressure
P_{00}	pressure at the bottom surface (1000 mb)

The variables are nondimensionalized as follows: y by L, x by L/n, t by f_0^{-1}, ψ and τ by $L^2 f_0$, θ by $AL^2 f_0$, w by Hf_0, k_d, k'_d, h_d by f_0, σ by $AL^2 f_0$, and β_0 by $(Lf_0)^{-1}$. We now define the dimensionless constants $\beta \equiv La^{-1}\cot\varphi_0$, $\sigma_0 \equiv \sigma(AL^2 f_0)^{-1}$, $2k \equiv k_d f_0^{-1}$, $k' \equiv k'_d f_0^{-1}$, and $2h'' \equiv h'_d f_0^{-1}$. Note that in a dimensionless channel of width π and zonal length 2π, L is a length scale related to the meridional channel width, L_y, and zonal circle length, L_x, by $L_y = \pi L$ and $L_x = 2\pi L/n$. The parameter n is the aspect ratio of the horizontal length scales. Specifically, $n = 2L_y/L_x$. Choosing n different from one redefines the fundamental harmonic. For example, $n = 1$ gives a period of $2\pi L = L_x$ whereas $n = 0.5$ scales the fundamental period to $4\pi L = L_x$.

The dependent variables are expanded in the orthonormal eigenfunctions, F_i, of the Laplace operator. These eigenfunctions satisfy the following conditions:

$$\nabla^2 F_i = a_i^2 F_i$$

$$\frac{\partial F_i}{\partial x} = 0 \quad \text{at} \quad y = 0, \pi$$

$$\overline{F_i F_j} = \delta_{ij},$$

where

$$\overline{(\ )} \equiv \frac{\int_0^\pi \int_0^{2\pi} (\ )\,dx\,dy}{\int_0^\pi \int_0^{2\pi} dx\,dy}$$

is the horizontal average of ( ), and δ_{ij} is the Kronecker delta function. The eigenfunctions chosen include the families

$$f_{A(P_i)} = \sqrt{2}\cos(P_i y)$$

$$f_{K(M_j,P_j)} = 2\cos(M_j x)\sin(P_j y)$$

$$f_{L(H_j,P_j)} = 2\sin(H_j x)\sin(P_j y),$$

where $P_i = 1, 2, \cdots, Y_T$; $M_j = 1, 2, \cdots, X_T$; $H_j = 1, 2, \cdots, X_T$; and Y_T and X_T are the y and x wavenumbers, respectively, at which the expansion is truncated. The dimension of the resulting system of equations is $2Y_T(2X_T + 1)$, and the total number of eigenfunctions is $I_{eig} = Y_T(2X_T + 1)$. The above form of the eigenfunctions is slightly different in appearance from that used by Lorenz (1960, 1963), CS and RP. The argument of the ith harmonic in x is, in our case, "ix". In the aforesaid works the argument is "inx". This difference is due solely to a different choice of scaling for x. Our nondimensional x has absorbed the horizontal aspect ratio, n.

The expansions of the dependent variables thus take the form

$$\psi(x,y,t) = \sum_{P_i=1}^{Y_T} \psi_{A(P_i)}(t) f_{A(P_i)}(y) + \sum_{M_i=H_i=1}^{X_T} \sum_{P_i=1}^{Y_T} [\psi_{K(M_i,P_i)}(t) f_{K(M_i,P_i)}(x,y) + \psi_{L(H_i,P_i)}(t) f_{L(H_i,P_i)}(x,y)]$$

$$\tau(x,y,t) = \sum_{P_i=1}^{Y_T} \tau_{A(P_i)}(t) f_{A(P_i)}(y) + \sum_{M_i=H_i=1}^{X_T} \sum_{P_i=1}^{Y_T} [\tau_{K(M_i,P_i)}(t) f_{K(M_i,P_i)}(x,y) + \tau_{L(H_i,P_i)}(t) f_{L(H_i,P_i)}(x,y)]$$

$$\theta(x,y,t) = \sum_{P_i=1}^{Y_T} \theta_{A(P_i)}(t) f_{A(P_i)}(y) + \sum_{M_i=H_i=1}^{X_T} \sum_{P_i=1}^{Y_T} [\theta_{K(M_i,P_i)}(t) f_{K(M_i,P_i)}(x,y) + \theta_{L(H_i,P_i)}(t) f_{L(H_i,P_i)}(x,y)]$$

$$\theta^*(x,y) = \sum_{P_i=1}^{Y_T} \theta^*_{A(P_i)} f_{A(P_i)}(y) + \sum_{M_i=H_i=1}^{X_T} \sum_{P_i=1}^{Y_T} [\theta^*_{K(M_i,P_i)} f_{K(M_i,P_i)}(x,y) + \theta^*_{L(H_i,P_i)} f_{L(H_i,P_i)}(x,y)]$$

$$w(x,y,t) = -\sum_{P_i=1}^{Y_T} \omega_{A(P_i)}(t) f_{A(P_i)}(y) - \sum_{M_i=H_i=1}^{X_T} \sum_{P_i=1}^{Y_T} [\omega_{K(M_i,P_i)}(t) f_{K(M_i,P_i)}(x,y) + \omega_{L(H_i,P_i)} f_{L(H_i,P_i)}(x,y)]$$

$$h(x,y) = \sum_{P_j=1}^{Y_T} h_{A(P_i)} f_{A(P_i)}(y) + \sum_{M_i=H_i=1}^{X_T} \sum_{P_i=1}^{Y_T} [h_{K(M_i,P_i)} f_{K(M_i,P_i)}(x,y) + h_{L(H_i,P_i)} f_{L(H_i,P_i)}(x,y)].$$

The Jacobian terms in the model equations are also expanded,

$$J(F_j, F_m) = \sum_i c_{ijm} F_i,$$

where c_{ijm} are interaction coefficients defined by

$$c_{ijm} \equiv \overline{F_i J(F_j, F_m)}.$$

Depending on which family of eigenfunctions F_i is a member of, the 'Σ' sign above represents summation over one index (if $F_i \in \{f_A\}$) or summation over two indices (if $F_i \in \{f_K, f_L\}$). It follows from the properties of the Jacobian that $c_{ijm} = -c_{imj}$, and from the boundary conditions on the channel walls that $c_{ijm} = c_{jmi} = c_{mij}$. General formulas for the interaction coefficients are given in appendix A. For completeness we note that the expansion of the β-term uses the relation $\partial F_m/\partial x = \sum_i b_{im} F_i$, where $b_{im} \equiv \overline{F_i(\partial F_m/\partial x)}$ (see appendix A).

The final nondimensional, spectrally decomposed equations are

$$\frac{\partial}{\partial t}\psi_i = \frac{n}{2} a_i^{-2} \sum_j^N \sum_m^N c_{ijm}\{(a_j^2 - a_m^2)(\psi_j\psi_m + \theta_j\theta_m) + h_m(\psi_j - \theta_j)\} + n\beta a_i^{-2} \sum_j^N b_{ij}\psi_j - k(\psi_i - \theta_i) \quad (2.5)$$

$$\frac{\partial}{\partial t}\theta_i = \frac{n}{2} a_i^{-2} \sum_j^N \sum_m^N c_{ijm}\{(a_i^2 - a_m^2)(\theta_m\psi_j + \theta_j\psi_m) - h_m(\psi_j - \theta_j)\} + n\beta a_i^{-2} \sum_j^N b_{ij}\theta_j + k(\psi_i - \theta_i) - 2k'\theta_i - a_i^{-2}\omega_i \quad (2.6)$$

$$\frac{\partial}{\partial t}\theta_i = -n \sum_j^N \sum_m^{N'} c_{ijm}\psi_j\theta_m + \sigma_0\omega_i + h''(\theta_i^* - \theta_i). \quad (2.7)$$

Here the subscripts i, j and m refer to an ordering of all eigenfunctions, F_i, $i = 1, 2, \cdots, I_{eig}$. Eliminating ω_i by combining Eqs. (2.6) and (2.7) results in a system

of nonlinear ordinary differential equations for the variables $\psi_i(t)$ and $\theta_i(t)$.

As in CS and RP, the thermal forcing is represented by a single zonal component

$$\theta^*(x, y) = \theta^*_{A(1)}\sqrt{2}\cos(y) = \theta^*_A\sqrt{2}\cos(y),$$

and the topographic forcing is represented by a single wave component

$$h(x, y) = h_{k(1,1)}2\cos(x)\sin(y) = h_K 2\cos(x)\sin(y).$$

Due to this choice of forcing, the large-scale waves (i.e., those of zonal wavenumber 1) are the only directly forced waves. All other waves are indirectly forced via instabilities and nonlinear interactions.

There is a fair amount of freedom in deciding what values to assign to the model parameters (see Reinhold, 1981). In the present paper, we choose to adopt the set from RP's demonstration case to facilitate comparisons with that work. The scaling constants in this set are $\varphi_0 = 50°\text{N}$, $L = 1600$ km (a channel width of $\pi L = 5000$ km), $a_0 = 6400$ km, $H \approx 7.5$ km, $f_0 = 1 \times 10^{-4}$ s^{-1}, and $A = 1.1886 \times 10^{-10}$ s °K/cm^2. The model parameters take on the values $\beta = 0.2$, $\sigma_0 = 0.1$, $h_K = 0.2$, $k = 0.5$, $k' = 0.01$, $h'' = 0.045$, $\theta^*_A = 0.1$, and $n = 1.3$. A study of this model under different parameter regimes will appear in Part III.

3. Low-order versus high-order models

In adopting low-order dynamical systems to model the original governing partial differential equations, one inevitably makes errors. However, it is often assumed that the qualitative behavior of the full system is essentially captured by the truncated system and that as more and more modes are included, the accuracy of the approximation will gradually improve. As we will show, this is not necessarily the case for the two-layer model under consideration. Whether or not a low-order system can at least qualitatively approximate the behavior of the full system depends critically on whether or not the various significant modes of nonlinear interaction inherent in the full system are included.

For barotropic models, an important form of nonlinear interaction is between waves and the mean shear (Davey, 1980, 1981; Rambaldi and Mo, 1984; Tung and Rosenthal, 1985). If this interaction is "truncated away," as in the model of Charney et al. (1981), the solution of the truncated system will bear no resemblance to the full (converged) system in some respects. This has been shown in Part I by Tung and Rosenthal (1985) with regard to the presence of multiple equilibria.

In baroclinic models, the presence of vigorous self-excited baroclinic instability greatly complicates the forms of significant interactions that need to be incorporated. In models with stationary forcing at the large scales and self-excited free waves at the synoptic scales, the various forms of nonlinear interactions are the following: forced wave–mean flow interaction, free wave–mean flow interaction, forced wave–free wave and free wave–free wave interactions.

Charney and Straus (1980) truncated their spectral expansion at $1x$- and $2y$-modes, resulting in a system with 12 degrees of freedom. The only nonlinear interactions present at this level are between the waves and the mean flow. By retaining an additional x-mode in the synoptic scale, the $2x$-, $2y$-system (with 20 degrees of freedom) of RP allowed for the excitation of highly unstable, synoptic-scale waves. The interactions afforded by this additional scale were found to greatly alter the variability of the forced waves by introducing a significant chaotic component in the time-dependent behavior of these large-scale waves. What is left out of the model, at the level of truncation adopted by RP, are interactions among the free waves, i.e., waves not directly forced by topography. It may at first appear that as long as one is mainly interested in the behavior of the large-scale forced waves this deficiency involving the self-excited waves themselves would only be of secondary importance. What has not been taken into account is the important role played by the wave–wave interactions among the intermediate and small scales in providing a path for vorticity cascade to the small scales, where significant dissipative sinks are usually present (see Salmon, 1978; Orszag and Kells, 1980; Marcus, 1981; Curry et al., 1984). Without proper channels for energy and vorticity cascades, a truncated system, such as that of RP, reverberates with interactions between the directly forced large scales and the baroclinically excited synoptic scales. This produces exaggerated time-dependent variability in the large-scale waves and a very large excitation in waves at the wavenumber cutoff. Such behavior is referred to as "spurious chaos." This will be demonstrated as we reexamine the hierarchy of truncated two-layer models.

a. The model of Charney and Straus (1980)

In CS, as in all subsequent models we will discuss here, topographic elevation takes the form of one single zonal wavenumber harmonic at the planetary scale, the largest scale in the model:

$$h(x, y) = h_0\cos(x)\sin(y).$$

Only this single zonal wavenumber is also kept in their truncated solution. In the meridional direction, the first as well as the second harmonic is retained. This $1x$-, $2y$-system has six eigenfunctions; the resulting system of real ordinary differential equations is 12-dimensional.

Charney and Straus noted that if all of the second y-mode amplitudes were initially zero, then they would remain zero for all time. Thus a simpler, 6-dimensional system satisfies the 12-dimensional system of equations. This more severely truncated model of $1x$- and $1y$-modes incorporates the rudiments of forced wave–zonal flow interaction. Including a second y-mode allowed CS to determine the effects of an additional

meridional mode; in particular, it enabled them to ascertain the relevance of a low-order model ($1x$-, $1y$-modes) to one of slightly higher resolution ($1x$-, $2y$-modes).

Charney and Straus solved for equilibrium solutions of the ($1x$, $1y$) subsystem, that is, equilibria of the largest scale. For sufficiently strong thermal forcing, θ_A^*, they found a multiplicity of equilibrium solutions. For one set of parameter values with $0 < \theta_A^* < 0.131$, only the Hadley solution existed. This purely zonal circulation has no flow in the bottom layer and hence does not interact with the topography. All wave components are zero. At $\theta_A^* = 0.135$, corresponding to a 72°K temperature difference across the channel at radiative equilibrium, two more equilibria appeared. Since these solutions have nonzero wave components they were called wavey equilibria. A limit point was encountered at $\theta_A^* \approx 0.18$ beyond which a total of five steady-state solutions were found. This forcing corresponds to a 95°K temperature difference across the channel. At this strong driving there exist both high and low zonal index solutions. The low zonal index equilibrium is stable with respect to first y-mode perturbations. As the name suggests, it resembles a low-index blocking state with a relatively weak zonal flow and a strong wave component. The other four equilibria are unstable to perturbations of the first y-mode variables.

The behavior of the six equation system is summarized in Fig. 1. Figures 1a–f are the bifurcation diagrams of the six variables as a function of the radiative forcing, θ_A^*. The value of θ_A^* ranges from 0.0 to 0.12, or 0 K–100 K. The solid lines denote stable points, and the solid and unfilled circles denote unstable points of the stationary and propagating types of instabilities, respectively. To facilitate later comparisons, the parameter values used here were those of RP's demonstration case. As seen in the diagrams, there is only one equilibrium solution, the purely zonal Hadley solution, for $0 < \theta_A^* < 0.0679$. The Hadley solution is stable in this range of θ_A^* and describes the only type of behavior that the ($1x$, $1y$) model is capable of. At $\theta_A^* = 0.0679$ (i.e., 58°K temperature difference) there is a bifurcation point. The Hadley solution is unstable for $\theta_A^* > 0.0679$. The time-dependent solution now converges to one of the two new equilibria. One of these steady state solutions has a westerly flow in the lower layer (referred to as the branch 1 equilibrium by CS). The other has lower layer easterlies (referred to as the branch 2 solution by CS). A limit point is encountered at $\theta_A^* = 0.0835$, or 72 K. For $\theta_A^* > 0.0835$ there are five equilibria. (These two new solution branches were called the branch 3 and branch 4 solutions by CS.) Charney and Straus pointed out that for sufficiently strong thermal driving, only the branch 1, low-index, blocking solution is stable to perturbations of the first y-mode variables. This behavior is depicted in Fig. 2 for $\theta_A^* = 0.1$. Figure 2 shows the various trajectories followed by the system when it is perturbed about each of the five equilibria. This is a phase space plot of the mean streamfunction wave amplitudes, ψ_K versus ψ_L, where $\psi_K \equiv \psi_{K(1,1)}$ and $\psi_L \equiv \psi_{L(1,1)}$. [Hereafter the wavenumbers will be dropped from the largest scale ($1x$, $1y$) components. The variables ψ_A, ψ_K, ψ_L, θ_A, θ_K, θ_L now correspond exactly to the notation of CS.] These are the cos$x$- and sin$x$-components, respectively, of the largest scale waves, which are directly forced by topography. The stable point to which all trajectories lead is the low-index blocking state of CS; RP called this equilibrium the 45° trough solution. (RP labeled three of the equilibria according to their relative phase with respect to the topography: 45° trough, 90° ridge, 30° ridge. The other two equilibria were called the Hadley and the near Hadley solutions.)

It should be noted here that the response of this model can change, depending on the initial conditions, on the parameter values, and on the number of modes. Indeed, in the full CS model of $1x$-, $2y$-modes, all of the equilibria are unstable to the second y-mode. The time-dependent response leads to either periodic or aperiodic behavior. Nonetheless, CS suggested that a transition to blocking could occur as a result of instability.

b. *The model of Reinhold and Pierrehumbert (1982)*

Reinhold and Pierrehumbert extended the CS model to include a second mode in x. With $2x$- and $2y$-modes the dimension of the system of equations is now 20. The addition of a second x-mode introduces highly baroclinically unstable waves into the model, which give rise to several new types of nonlinear interactions. Charney and Straus did not address the importance of the smaller scale free waves except to postulate that they aided in the transition process from one equilibrium point to another. The new mechanism that RP introduced proved to be of major importance.

Once again, the six-equation system described above is a subsystem of this higher order model. That is to say, if the amplitudes of all second x- and y-mode components are initially zero, they will remain zero. Thus the large-scale equilibria of the $1x$-, $1y$-mode system also satisfy the ($2x$, $2y$) model of RP. However, these large-scale equilibria turn out to be highly unstable to perturbations of the synoptic-scale, free waves. In Fig. 3 we see the effect of perturbing the 20-variable system from the Hadley equilibrium and integrating for a period of 414 days. As in Fig. 2, this is a phase space plot of the amplitudes of the topographically forced, large-scale wave components, ψ_K and ψ_L. For this run all amplitudes, except for ψ_A and θ_A (the Hadley solution), were perturbed. This initialization is not crucial, though. A slight perturbation from the 45° trough, low-index blocking solution produces a similar result (Fig. 4). The effect of the self-excited waves is visibly drastic. Where there was orderly behavior in the ($1x$, $1y$) model, there is chaotic motion in the RP

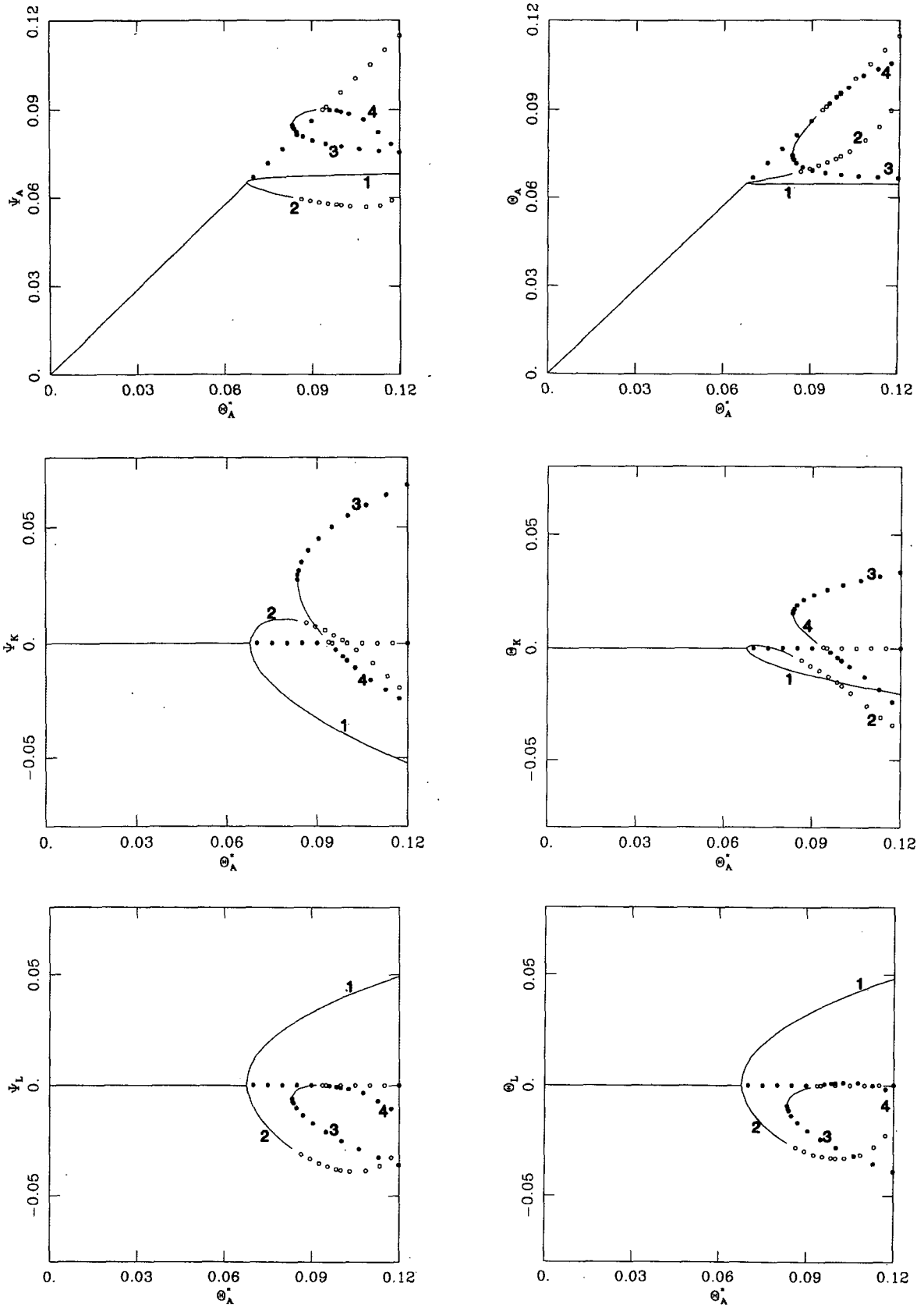

FIG. 1. Bifurcation diagrams of the 6 ($1x$, $1y$) model variables as functions of θ_A^*. The solid lines denote stable points. The solid and unfilled circles denote unstable points of the stationary and propagating types of instabilities, respectively. 1, 2, 3, 4 refer to the branch number.

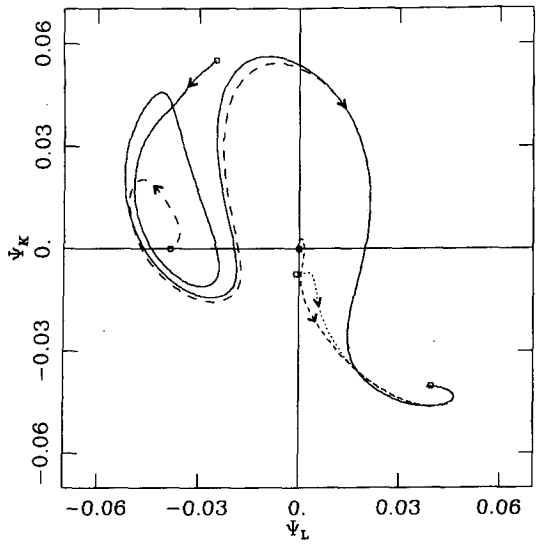

FIG. 2. Phase space trajectories of components ψ_K and ψ_L of the 1x-, 1y-system when perturbed about each of five equilibrium points. The equilibria are marked with a square.

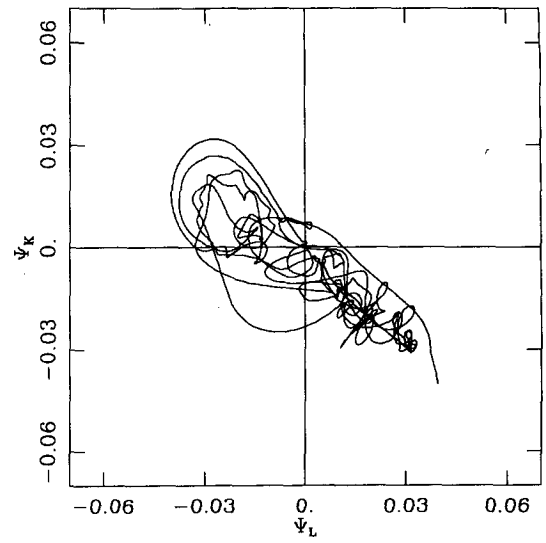

FIG. 4. As in Fig. 3 except that the system is perturbed from the 45° trough equilibrium point.

model. The relevance of the large-scale equilibria is not obvious here.

Reinhold and Pierrehumbert postulated the existence of weather regimes. Weather regimes are periods of "quasi-stationary behavior in the large scales associated with organized behavior of the synoptic scales." Figure 3 shows the two basic regime states: the ridge regime in the second quadrant and the trough regime in the fourth quadrant. Blocking was theorized to be one type of behavior observed in the trough regime. In the (2x, 2y) model, RP found that the synoptic scale

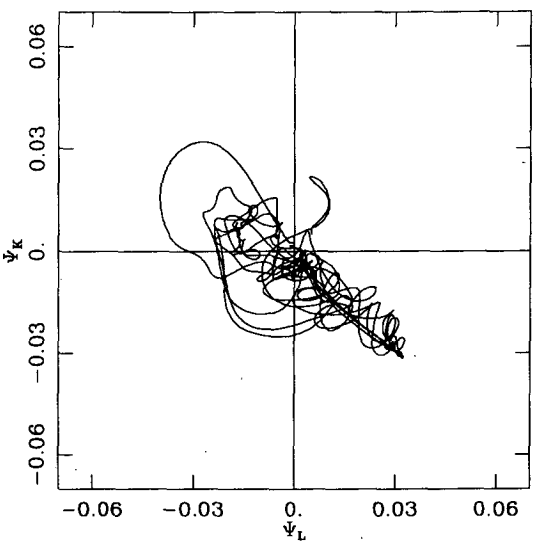

FIG. 3. Phase space trajectory of components ψ_K and ψ_L of the 2x-, 2y-system when perturbed from the Hadley equilibrium (time steps 0–4000).

disturbances both acted as a forcing on and maintained the large-scale flow.

c. *Problems with the old models*

There are, however, certain problems inherent in the models of CS and RP. The RP model is often viewed as a correction to the CS model. A second mode in x was included above that of the CS model, which meant that the spectral resolution of the RP model was slightly higher. Reinhold and Pierrehumbert modified the CS multiple equilibria theory to incorporate new effects due to this additional mode. The attractor that RP found was a drastic change from the response of the CS model. Reinhold and Pierrehumbert thereby showed that the synoptic waves play a major role in the model response. It is important to ask at this point whether all mechanisms are accounted for in the model: Are there still some interactions missing? To be sure, this leads to questions of convergence. In Fig. 5 the response of the smallest scale of the RP model is plotted. The amplitude of the smallest scale is actually larger than that of the largest scale. Table 1 gives the bounds of the components plotted in Figs. 3 and 5. With such a large excitation in the smallest scales it is evident that the model is not yet converging. Furthermore, as pointed out by Curry et al. (1984), large excitations near the wavenumber cutoff are indicative of spurious chaos. This suggests that keeping more modes may cause the random motion to largely disappear.

The model equations have a quadratic nonlinearity. From a physical point of view this supports several types of interactions. The interactions may involve the zonal flow, large-scale waves directly forced by topography, and free waves, i.e., those not directly forced by

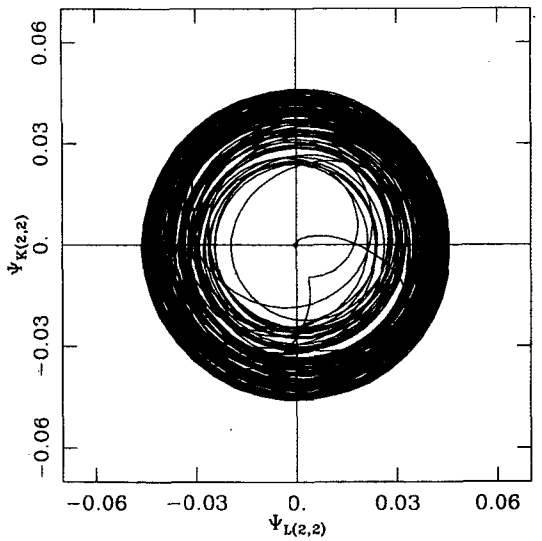

FIG. 5. Phase space trajectory of the smallest-scale components of the $2x$-, $2y$-system, $\psi_{K(2,2)}$ versus $\psi_{L(2,2)}$. The system was perturbed from the Hadley equilibrium and integrated for 4000 time steps.

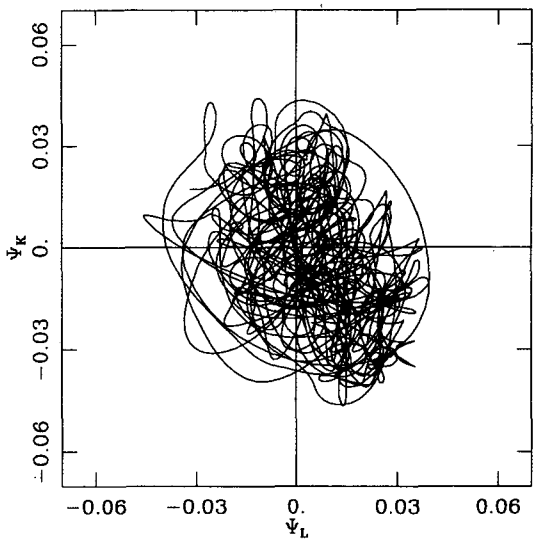

FIG. 6. Phase space trajectory of components ψ_K and ψ_L of the $3x$-, $2y$-system (random initialization, 4000 time steps).

topography. As stated earlier, the ($1x$, $1y$) model supports two types of nonlinear interactions:

1) the self-interaction of two waves forced by topography modifying the zonal flow, and

2) the interaction between the zonal flow and one wave forced by topography modifying another wave of the same scale.

The RP model, which includes a highly baroclinically unstable wave, gives rise to several new interactions. These were observed to introduce a significant chaotic component into the low-frequency response of the model.

At the $3x$-, $2y$-truncation level there are triad interactions between the $1x$, $2x$ and $3x$ waves, and all waves interact with the topography (Yoden, 1983b). The effect of this new triad interaction is impressive, as seen in Fig. 6. The response of the system is very chaotic. The circularity of the ridge regime and the linearity of the trough regime are no longer present. Instead, there is a highly random behavior, contained mainly in the fourth quadrant, that spreads into the other quadrants. It is evident that the third x-mode in some sense has a destabilizing influence on the large-scale components.

TABLE 1. Bounds of the largest and smallest scale mean streamfunction components of the $2x$-, $2y$-system. The system was perturbed from the Hadley equilibrium and integrated for 4000 time steps.

RP model
$-0.0316 \leqslant \psi_K \leqslant 0.0321$
$-0.0398 \leqslant \psi_L \leqslant 0.0327$
$-0.0458 \leqslant \psi_{K(2,2)} \leqslant 0.0462$
$-0.0461 \leqslant \psi_{L(2,2)} \leqslant 0.0458$

To further understand the importance of the interaction betwen the $1x$, $2x$ and $3x$ waves, these triads were removed and the system was integrated in time as before. Figure 7 shows the results of this experiment. The similarity of this phase plot to that of RP's (Fig. 4) is quite striking both qualitatively and quantitatively. Once again the trough and ridge regimes are present. The $2x$-, $2y$-components are shown in Fig. 8. Figure 8a shows the response of the full $3x$-, $2y$-system, while Fig. 8b demonstrates the case in which the triad interactions among the $1x$, $2x$ and $3x$ waves were suppressed. Comparing these plots with Fig. 5 (RP model) again illustrates that the no-triad case is almost identical

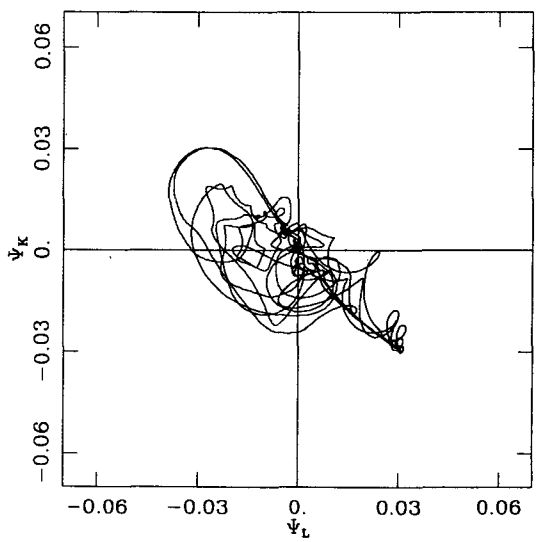

FIG. 7. As in Fig. 6 except that the triad interactions were removed.

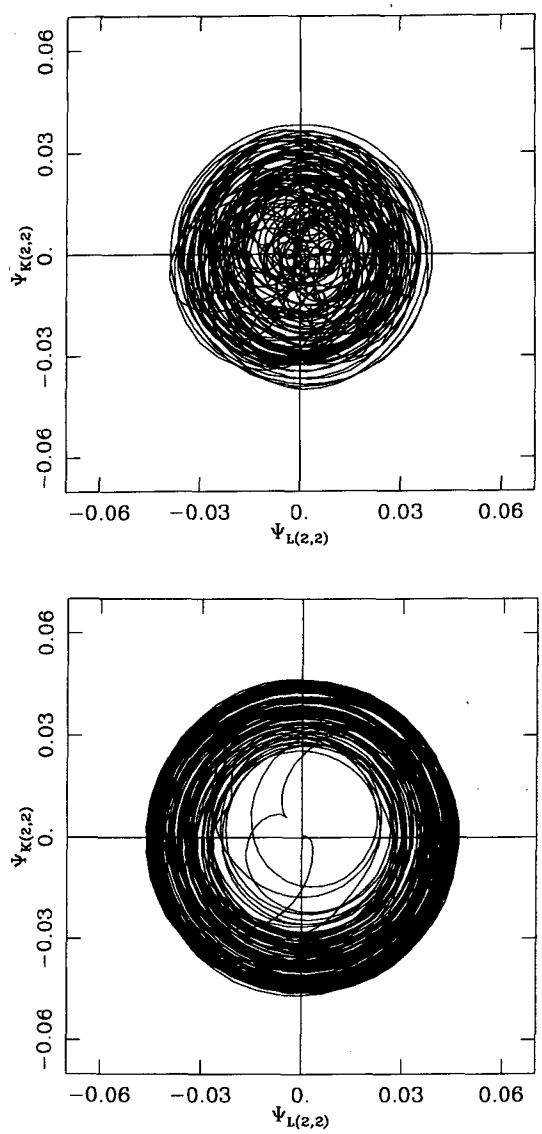

FIG. 8. Phase space trajectory of components $\psi_{K(2,2)}$ and $\psi_{L(2,2)}$ of the $3x$-, $2y$-system (random initialization, 4000 time steps). (a) The full $3x$-, $2y$-system. (b) The $3x$-, $2y$-system without triad interactions.

to the $(2x, 2y)$ model: there is virtually no resemblance to the full $3x$-, $2y$-system.

The $(3x, 2y)$ model gives an excellent demonstration of the role that certain nonlinear interactions play in providing a path for vorticity cascades to the smaller scales. Table 2 lists the bounds of the $(1x, 1y)$, the $(2x, 2y)$ and the $(3x, 2y)$ components of the mean streamfunction from the time integrations of the $(3x, 2y)$ model. The results of the full $(3x, 2y)$ model show an overall decrease in amplitudes in going from the largest to the smallest scales. This is in contrast to what was found for the $(2x, 2y)$ model (see Table 1). If we now turn our attention to the bounds in Table 2 for the no-triad case, we see that this case differs sharply from the

TABLE 2. Bounds of the $(1x, 1y)$, $(2x, 2y)$ and $(3x, 2y)$ mean streamfunction components of the $(3x, 2y)$ model. (a) The full model. (b) The model without triad interactions among the $1x$, $2x$ and $3x$ waves.

(a)	
	$-0.0466 \leq \psi_K \leq 0.0442$
	$-0.0457 \leq \psi_L \leq 0.0395$
	$-0.0398 \leq \psi_{K(2,2)} \leq 0.0383$
	$-0.0391 \leq \psi_{L(2,2)} \leq 0.0393$
	$-0.0173 \leq \psi_{K(3,2)} \leq 0.0155$
	$-0.0139 \leq \psi_{L(3,2)} \leq 0.0147$
	$-0.0302 \leq \psi_K \leq 0.0304$
	$-0.0387 \leq \psi_L \leq 0.0322$
	$-0.0470 \leq \psi_{K(2,2)} \leq 0.0463$
	$-0.0464 \leq \psi_{L(2,2)} \leq 0.0468$
	$O(-10^{-10}) \leq \psi_{K(3,2)} \leq O(10^{-10})$*
	$O(-10^{-10}) \leq \psi_{L(3,2)} \leq O(10^{-9})$*

* The error tolerance for the time integration was 10^{-10}.

full $(3x, 2y)$ model but bears an uncanny resemblance to the values in Table 1 for the $(2x, 2y)$ model. The importance of these triads in the $(3x, 2y)$ model is now clear: they are responsible for transferring vorticity downscale. Without them the smallest scales attain negligible amplitudes at best.

Given the dramatic change in going from $2x$ to $3x$ modes, one is inclined to ask what effect other modes would have on the large-scale response. Figure 9 shows the time-integrated response of the $(4x, 2y)$ model. The change in the large-scale response due to the fourth x-mode is slight, at best. Including another mode in x does not appear to have further destabilized the flow.

Efforts thus far have concentrated on the effects of increasing the number of x-modes. It is interesting to

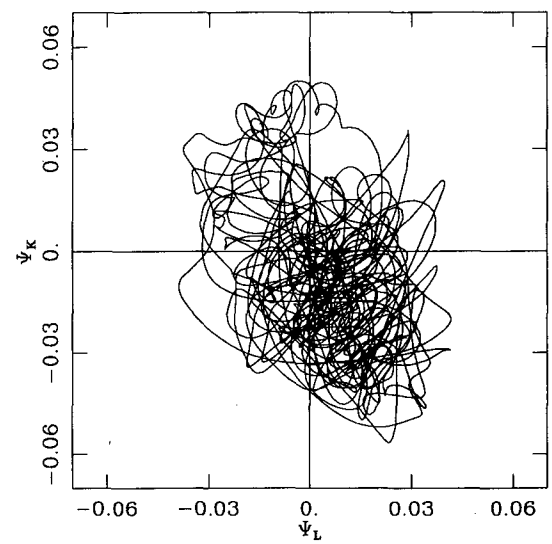

FIG. 9. Phase space trajectory of components ψ_K and ψ_L of the $4x$-, $2y$-system (random initialization, 4000 time steps).

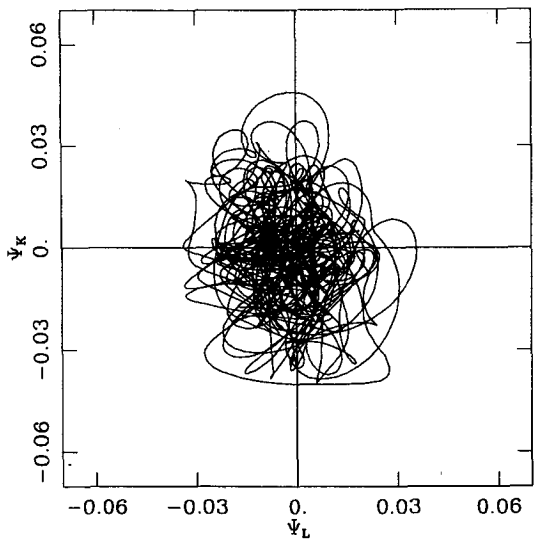

FIG. 10. Phase space trajectory of components ψ_K and ψ_L of the $2x$-, $3y$-system (random initialization, 4000 time steps).

see the effect of a third y-mode. Figure 10 is the result of integrating the $(2x, 3y)$ model. Again there is a dramatic difference between this response and that of the RP $(2x, 2y)$ model (Fig. 3). Not only have the regimes disappeared, but the activity of the chaotic attractor is more or less centered at the origin. This is in contrast to the response of the $(2x, 2y)$, $(3x, 2y)$ and $(4x, 2y)$ models, where the activity of the large-scale is contained mainly within the second and fourth quadrants. The third y-mode clearly plays a significant role in the model response as compared to the $2y$-models. This difference is probably related to the fact that the $(1x, 1y)$ model, which is a subsystem of the $(1x, 2y)$ and $(2x, 2y)$ models, is not a subsystem of the $(2x, 3y)$ model. Indeed, this is true of systems with three or more y-modes. This raises more questions as to the relevance of the large-scale equilibria to higher order models.

We have seen that changing the resolution in x and/or y can lead to significantly differing responses. How such intermediate levels of truncation compare with the "converged" model is a very important consideration. Figure 11 shows the effects of including higher numbers of modes in both x and y. Each model was initialized with a perturbation of every variable. Thus, a higher order model, which necessarily had more variables, was initialized with a greater number of nonzero variables than a model of lower resolution. When the modes are increased from $(3x, 3y)$ (Fig. 11a) to $(4x, 4y)$ (Fig. 11b) the features of the phase space plots change drastically. Whereas the $(3x, 3y)$ model response is somewhat rounded and centered near the origin, the $(4x, 4y)$ attractor is concentrated in a relatively well defined region in the fourth quadrant. The latter behavior persists for the $(5x, 5y)$, $(6x, 6y)$, $(7x, 7y)$ and $(10x, 10y)$ models depicted in Figs. 11c–f, respectively. (Note that Fig. 11f, i.e., the plot of the $(10x, 10y)$ model, is a scatter plot, with each dot corresponding to one day.) This result along with the fact that smaller scales have smaller amplitudes (see Table 3) suggests that the model has *qualitatively* converged at $7x$- and $7y$-modes. We would like to stress that "convergence" in the present paper is not used in the strict mathematical sense. Rather, the term describes the point at which there is no gross qualitative change in the behavior of the model. Even though the attractor is stable, it is to be expected that two trajectories with slightly different initial conditions will differ significantly after some time. Thus, we do not expect the converged $(10x, 10y)$ and the $(7x, 7y)$ models to agree quantitatively. This growth of errors simulates the unpredictable character of the observed atmosphere.

Several runs were made where an artificial damping term was included to see if the effect of the small scales on the large scales can be simulated as a damping on the intermediate scales. Figure 12 shows the results of this experiment for the $(2x, 2y)$ (Fig. 12a), $(3x, 3y)$ (Fig. 12b), $(4x, 4y)$ (Fig. 12c) and $(5x, 5y)$ (Fig. 12d) models. The artificial damping was of the form $\nu_A\nabla^6\psi$, with damping time $1/\nu_A$ taken to be 80 days. The ∇^6 operator acts to severely damp the smaller scales while having little effect on the largest scale. The effective damping time for the largest scale is 20 days. Compared with the 1-day Ekman damping time used in this parameter set, the effect of this new term on the large scales is minimal. (A discussion concerning the parameter values adopted in this study will be taken up in the conclusion. A study using realistic parameters will appear in Part III.) What is most striking in Fig. 12 is that already at $(4x, 4y)$ modes the response has settled down to an attractor in the fourth quadrant.

It is interesting to observe that convergence in the two-layer model appears to depend on a "proper balance" between two roles of the smaller scales. One role for proper energy and enstrophy cascades between the larger scales where the forcing is applied and the small scales where dissipative effects are strongest (i.e., in models with scale-selective dissipation. Note that even in models without scale-dependent dissipation, a higher resolution implies the presence of more scales at which energy and/or enstrophy is dissipated.) In models without such mechanisms, baroclinic effects tend to be overemphasized.

A less severe form of artificial damping, namely, a subgrid friction, was incorporated into the converged model to test against the occurrence of ultraviolet catastrophes. For this case a ∇^6 damping was imposed on waves of total wavenumber greater than or equal to $\sqrt{72}$ [e.g., $(5x, 7y)$, $(6x, 6y)$, $(7x, 7y)$] and on the smallest purely zonal components, $\psi_{A(7)}$ and $\theta_{A(7)}$. The results of this experiment, shown in Fig. 13, reaffirm the conclusions previously drawn from the model without subgrid friction.

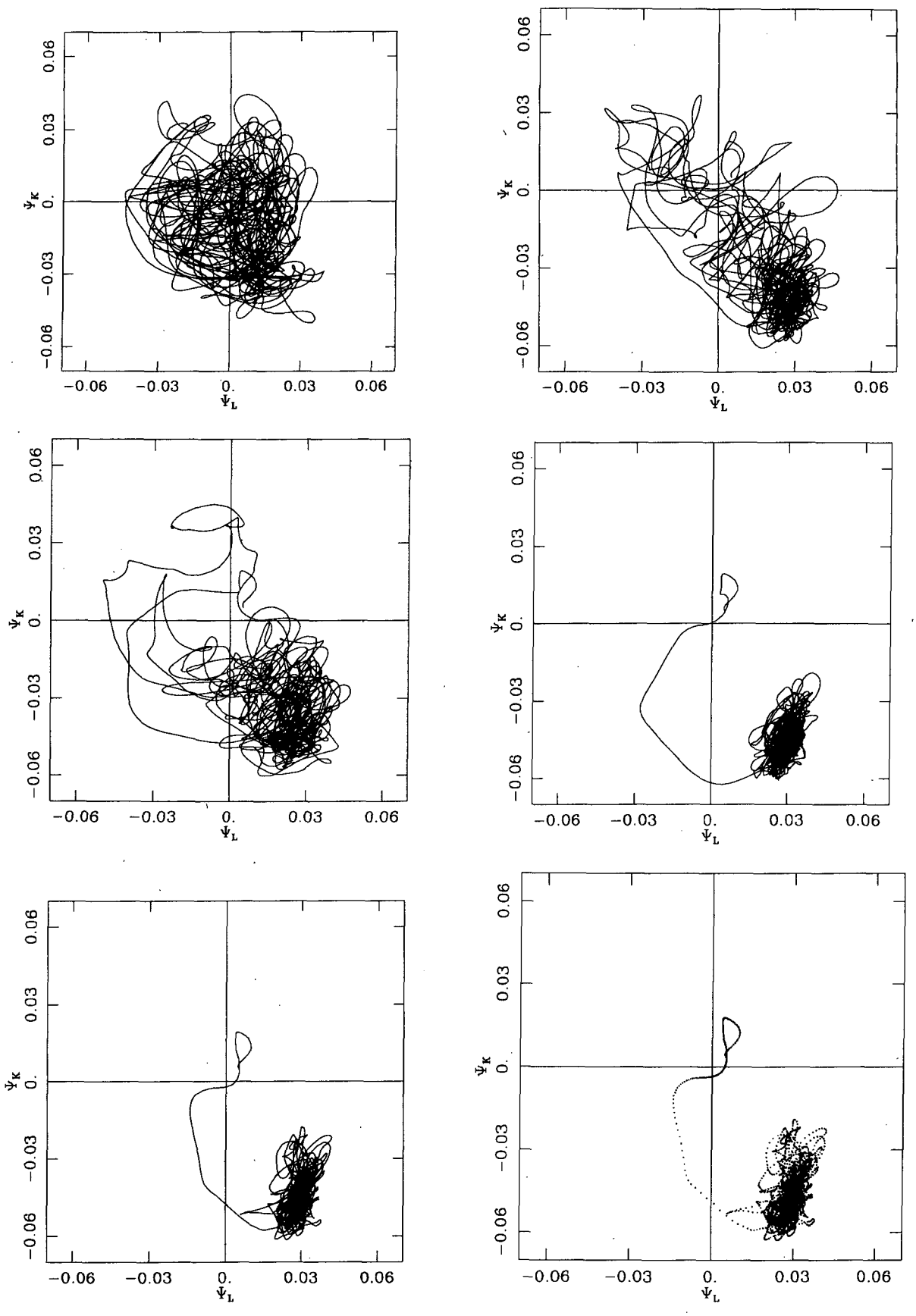

FIG. 11. Phase space trajectories of components ψ_K and ψ_L (random initialization, 4000 time steps). (a) 3x-, 3y-system, (b) 4x-, 4y-system, (c) 5x-, 5y-system, (d) 6x-, 6y-system, (e) 7x-, 7y-system, (f) 10x-, 10y-system (scatter plot).

TABLE 3. Bounds of the smallest scale mean streamfunction components of the 7x-, 7y-system. The system was initialized at a random point and integrated for 4000 time steps.

(7x, 7y) Model
$-4.89\times10^{-4}\leq\psi_{K(7,7)}\leq4.86\times10^{-4}$
$-4.96\times10^{-4}\leq\psi_{L(7,7)}\leq4.25\times10^{-4}$

d. Discussion

We have seen that, when both the destabilizing and dissipative effects of the synoptic scales on the large scales are incorporated, as in the converged case at the 7x-, 7y-level, the trajectory of the largest scale wave becomes less chaotic as compared with that obtained in lower-order models. Furthermore, the phenomenon of "multiple weather regimes" disappears. In its place there is only a single "weather regime," an attractor in the phase space of the large-scale waves. This attractor of the converged system is actually located near, i.e., it is similar in amplitude and phase to, the single stable, 45° trough low-index blocking state found in the six-component system of CS. It is remarkable how strikingly similar the persistent solution of the converged system, which incorporates the interaction among so many self-excited waves, is to the stable equilibrium of the truncated system, which excludes all scales except for the directly forced large-scale waves.

No other attractors (persistent weather regimes) ap-

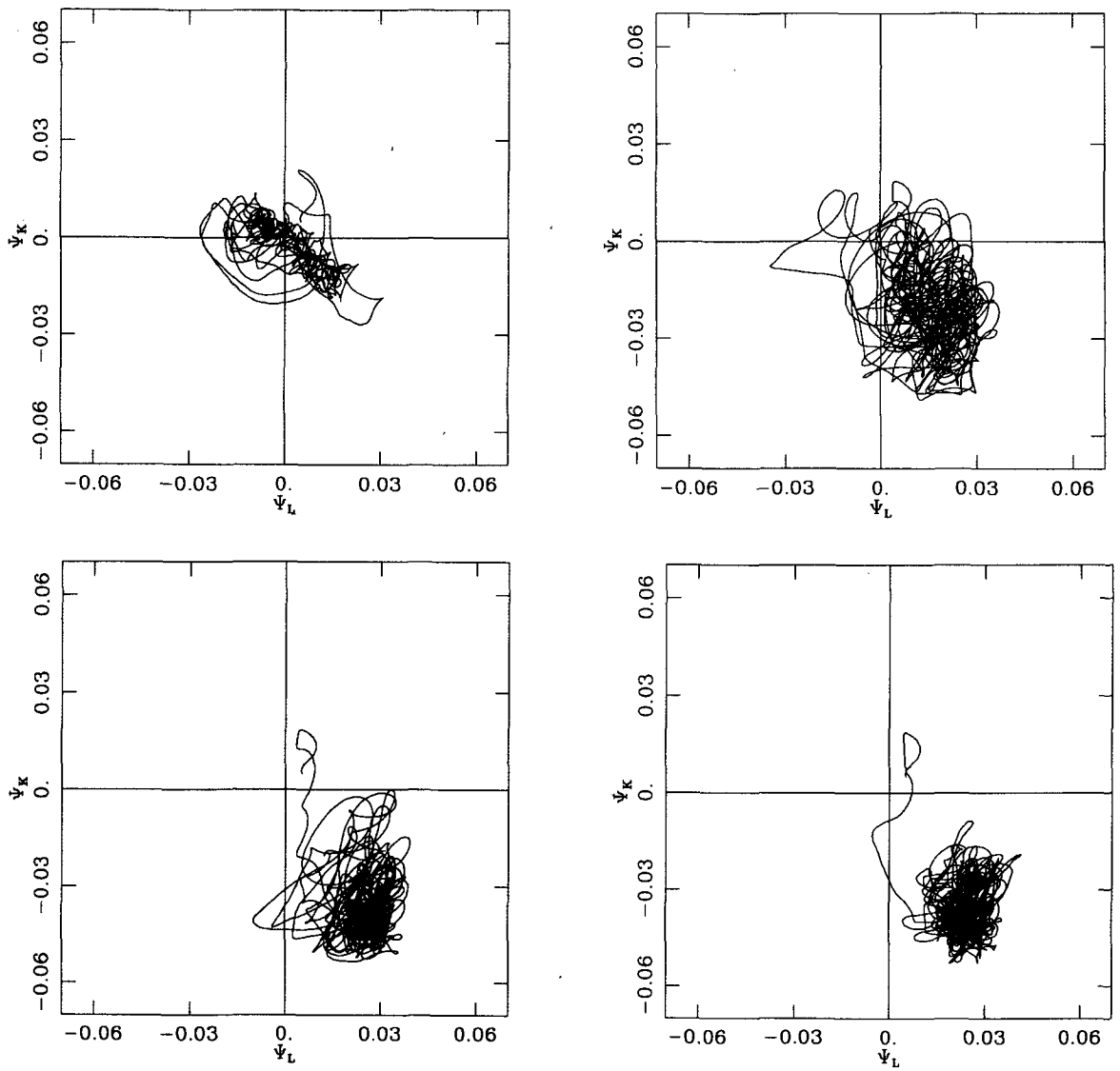

FIG. 12. Phase space trajectories of components ψ_K and ψ_L where artificial damping was used to hasten convergence (random initialization, 4000 time steps). (a) 2x-, 2y-system, (b) 3x-, 3y-system, (c) 4x-, 4y-system, (d) 5x-, 5y-system.

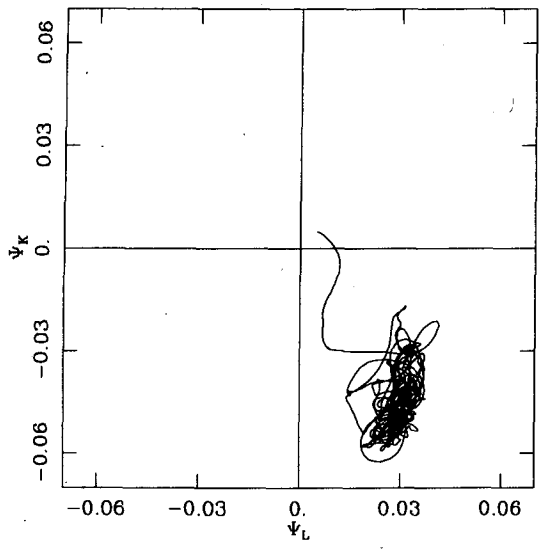

FIG. 13. Phase space trajectories of components ψ_K and ψ_L of the 7x-, 7y-system with subgrid friction (time steps 0–2000).

pear to exist. This is confirmed by performing several integrations of the converged system with various initial conditions. Examples are shown in Fig. 14. In all cases, the trajectories converged to the same single attractor in less than 20 days.

4. Single versus multiple weather regimes

Only a single weather regime is found in our full system in the same parameter range where RP found two. This is the same parameter range where 5 equilibria were found in the 1x-, 1y-system. Of the five equilibria, only one was found to be stable with respect to (1x, 1y) perturbations, and it is that stable equilibrium (45° trough, low index) which closely resembles the single weather regime in our converged solution. Charney and Straus, however, did not attach particular significance to the stability of the low-index solution, as it, along with the other four equilibria, was found to be unstable to (1x, 2y) perturbations. Instead, CS chose to treat both the low-index and the high-index equilibria as "meta-stable," with the instabilities playing the role of initiating the transition from one to the other equilibrium state.

The existence of only a single weather regime in our (fully nonlinear) solution presents a problem with regard to accounting for the observed variability of the atmosphere. Statistically, our solution is always in a low-index blocked state, with no persistent high index regimes. Either the present model is deficient in representing causes of variability in the atmosphere or there are other parameter ranges where multiple weather regimes can be found. The second possibility will be examined in this section (and in Part III), while the first will be pursued in sections 5 and 6.

Given the close resemblance between our solution and the stable equilibria of the 1x-, 1y-system, we find it helpful to organize our presentation using the bifurcation diagrams of the 1x-, 1y-system shown in Figure 1. In Fig. 15 results from the converged (7x, 7y) model were superimposed on the bifurcation diagrams of the (1x, 1y) model. This figure summarizes the responses of the two model resolutions as a function of thermal driving. For the converged model the markings are as follows: the "⊕" denote stable Hadley solutions, the "‡" marks a Hadley-like solution, i.e., wave amplitudes are negligible, and the vertical bars mark the bounds of a 30-day running time mean of the respective attractors. The markings for the (1x, 1y) model are as in Fig. 1.

At relatively low thermal driving, i.e., $0 < \theta_A^* < 0.0679$, the 1x-, 1y-system has only a single equilibrium point, the Hadley solution, which is stable to first x-, first y-mode perturbations. This is also the case for the fully nonlinear model but in a smaller range of thermal driving, $0 < \theta_A^* < 0.04$. This difference in behavior is due to the presence of the 2x wave. For this parameter set (more precisely, for $n = 1.3$) the only baroclinically unstable waves are the 1x and 2x waves. The 1x waves become unstable at $\theta_A^* = 0.0679$, while the 2x waves require a much smaller shear for growth, namely $\theta_A^* = 0.038$. For thermal driving in the range (0.04, 0.07) the 1x waves are baroclinically stable. It is because of the interaction of the unstable 2x waves with the large-scale (i.e., 1x scale) waves that the 1x waves attain small amplitudes in this range of driving (Fig. 15c–f). In either model, no multiple weather regimes were found for low values of thermal driving.

The (1x, 1y) model has a bifurcation point at θ_A^*

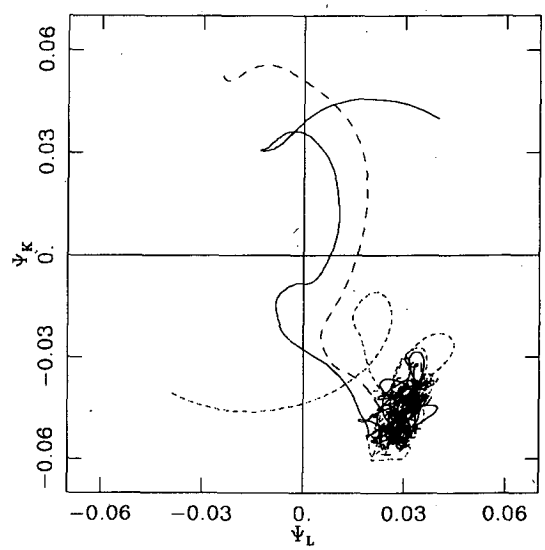

FIG. 14. Phase space trajectories of components ψ_K and ψ_L of the 7x-, 7y-system initialized in different regions of phase space (time steps 0–1000).

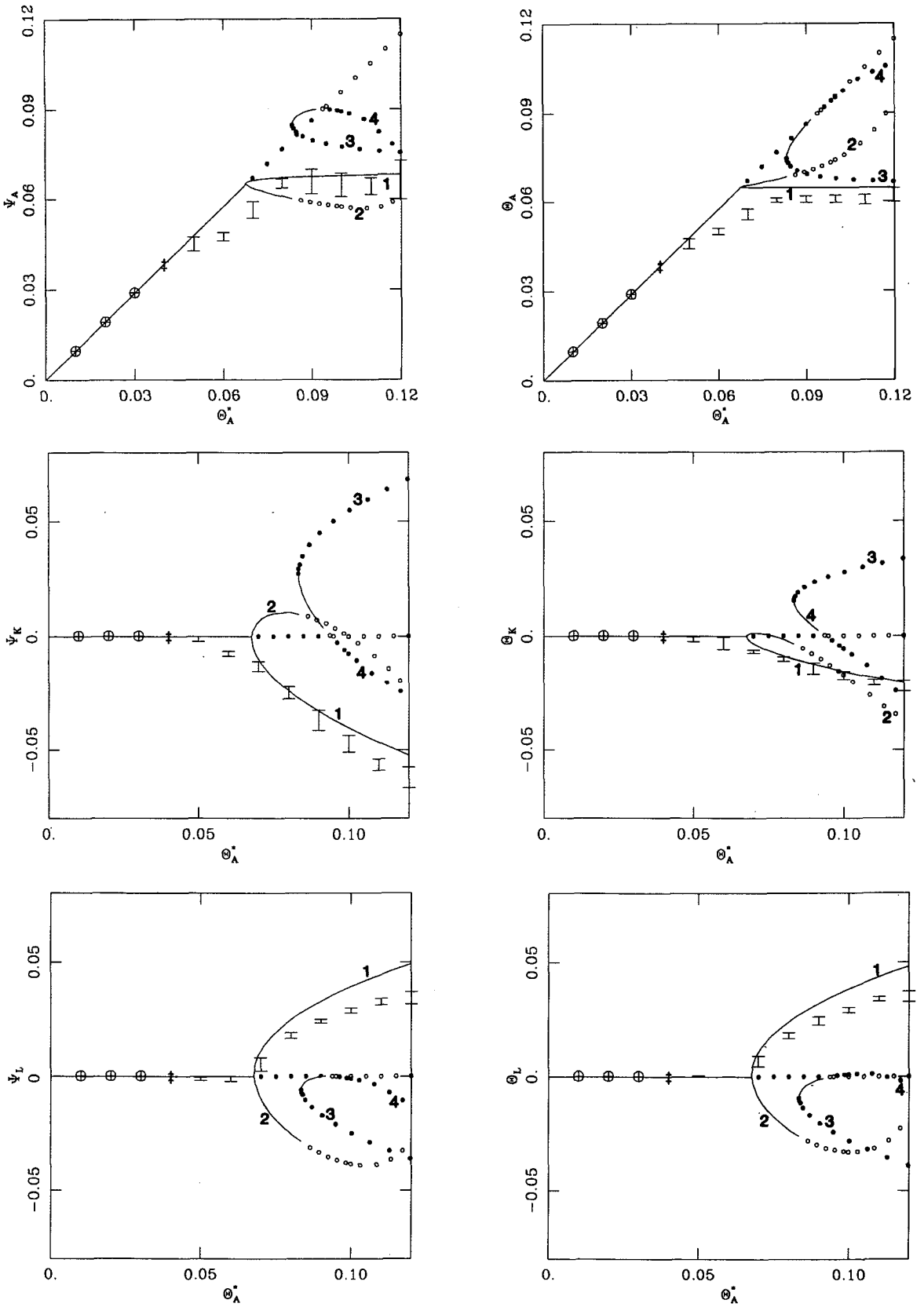

FIG. 15. Bifurcation diagrams of the 6 ($1x$, $1y$) model variables as functions of θ_A^*. The solid lines denote stable points. The solid and unfilled circles denote unstable points of the stationary and propagating types of instabilities, respectively. 1, 2, 3, 4 refer to the branch number. The response of the $7x$-, $7y$-system is marked as follows: the ⊕ mark the stable Hadley solutions, the '‡' marks a Hadley-like solution, i.e., wave amplitudes are negligible, and the vertical bars mark the bounds of a 30-day running time mean of the $7x$-, $7y$-system attractor over time steps 500–2000.

= 0.0679, beyond which the Hadley solution is unstable. For θ_A^* greater than this value, the $1x$ waves (in both models) are baroclinically unstable. In the range of moderate thermal driving, i.e., $0.0679 < \theta_A^* < 0.0835$, there are *two* stable wavy equilibria in the $1x$-, $1y$-system, the branch 1 and branch 2 solutions. Notice that both these branches are stable. Depending on the initial conditions, the model will converge to one or the other solution. These two points also have special stability properties in the full system. However, only one, the solution with a westerly flow in the lower layer (branch 1), develops into an attractor (and hence a weather regime). Again, only a single weather regime is found. That is, given any initial condition, the trajectory of the large-scale wave is eventually attracted to this single confined region in phase space. If the integration is initiated sufficiently close to the branch 2 equilibrium of the $1x$-, $1y$-system, the solution may linger at that point for about two months before being drawn toward the attractor with the lower level westerly. The significance of this (easterly) equilibrium is diminished by the fact that in the full system a solution initiated at any other point will not tend to it in later times. This situation is shown in Fig. 16.

In the parameter range of high thermal driving, $\theta_A^* > 0.0835$, there is only one single stable equilibrium of the $1x$-, $1y$-system and one single weather regime in the full system. In conclusion, we find only a single weather regime for all values of thermal driving.

The bifurcation diagram of θ_A versus θ_A^* (Fig. 15b) sheds much light on the importance of the branch 1 solution of the $(1x, 1y)$ model. Recall that it is this solution which bears close resemblance to that of the fully nonlinear model. The key feature of the branch 1 curve is its near linearity and, in particular, its almost constant value. That is to say, the zonal shear does not deviate significantly from its value at the bifurcation point $\theta_A^* = 0.0679$. Recall that it is at this critical point that the Hadley solution first becomes unstable in the $(1x, 1y)$ model. This is suggestive of an equilibration mechanism. Namely, there is a critical shear, θ_A, beyond which the Hadley solution is unstable. The system then supports a solution that maintains the shear near this critical level. This equilibration is accomplished through a growth in the wavy components of the flow field. An increase in thermal forcing is offset by an increase in eddy heat flux. The shear is thereby maintained at a nearly constant value. The dynamics governing the fully nonlinear model are more complex. This process will be studied in detail in a forthcoming paper. Here we offer a brief sketch. While it is true that the $2x$ waves become unstable at a much smaller shear than do the $1x$ waves, the model solution does not differ significantly from the Hadley solution in the range of driving where the $1x$ waves are stable. By this we mean that the largest scale components of the fully nonlinear model exhibit a response that is very close to the Hadley solution, in some averaged sense. It is not until $\theta_A^* > 0.0679$ that the solution begins to deviate significantly from the Hadley equilibrium. In this range of driving the $1x$ waves are unstable. The $2x$ waves become saturated, and the dynamics are governed by the largest scale, $(1x, 1y)$ waves. That is to say, increases in θ_A^* are mainly offset by increases in the largest scale waves. The most unstable $(2x)$ waves do not grow further in amplitude. Thus the fully nonlinear model behaves much like the branch 1 solution of the $(1x, 1y)$ model, equilibrating about a critical value of zonal shear. The main difference is the existence of a "branch" of weather regimes instead of equilibrium points. It is now not difficult to understand why the branch 1 solution is the only solution that is stable for all $\theta_A^* > 0.0679$ and why the only weather regime found in the fully nonlinear model is so similar to the branch 1 solution.

The RP model is interesting because it was thought to qualitatively model the atmosphere along with its observed, seemingly unpredictable weather patterns. An implication of the RP study is that the atmosphere can switch weather regimes purely as a result of *internal* nonlinear interactions without any change in "external" forcing. This feature is absence in our full system, implying that the time mean behavior of the large scales cannot change significantly in the absence of changes in external factors. How changes in "external" forcing can affect the single weather regime will be discussed in section 6. Next, in section 5 we shall discuss the energetics of the two-layer model used so far. This will point to a deficiency in its formulation that results in the exclusion of an important "external" cause of low-frequency variability of the large scales.

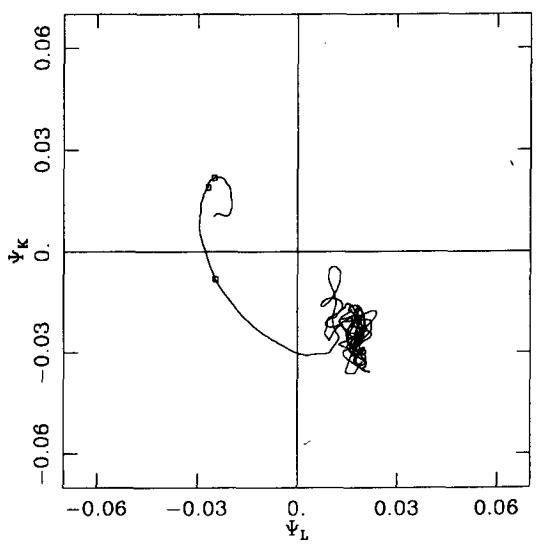

FIG. 16. Phase space trajectory of components ψ_K and ψ_L of the $7x$-, $7y$-system for $\theta_A^* = 0.08$. The model was perturbed from the branch 2 equilibrium of the $1x$-, $1y$-system and integrated for 2000 time steps. The squares mark periods of 30 days.

5. Baroclinic versus barotropic energy conversion

The models discussed thus far share a common feature. They are formulated for a midlatitude channel with rigid lateral boundaries. This produces a peculiarity in the momentum budget and, indirectly, in the energy budget of the model solution. As pointed out by Rambaldi (1982), Källén (1983) and Tung and Rosenthal (1985, 1986), what is missing in the formulation for the two-layer models is a momentum source for the flow in the midlatitude region. In the real atmosphere, the low-level flow north of 30°N has a net westerly momentum. From a diagnostic point of view, this net westerly momentum budget is accounted for mainly by the lateral flux of westerly momentum from the tropics. (The lateral transport is accomplished in part by the *equatorward* flux of *easterly* momentum carried by the stationary waves, and to a lesser degree by the northward advection of mean zonal momentum by the Hadley circulation and the northward flux of westerly momentum by the equatorial waves.)

In the absence of a momentum source for the two-layer model, CS found the energetics of their system to be drastically different from the energetics of the barotropic model considered by Charney and DeVore (1979) (hereafter referred to as CD), which did have a momentum forcing in the form of ψ^*. (Ironically, ψ^* was regarded by CD to be of "thermal" origin.) One would expect the generation of stationary waves by zonal flow over topography to be achieved via a transfer of zonal kinetic to eddy kinetic energy, as was the case in CD. Instead, for lower values of the driving θ_A^*, CS found such exchanges to be negligible. Furthermore, for higher thermal driving, the small orographic exchange always draws energy *from* the wave (see CS Fig. 8). Charney and Straus thus concluded that "orographic interactions play only an indirect role in the formation of wavy equilibria: they are a catalyst; they permit the equilibria to exist, but they do not directly support the stationary waves. The latter obtain their energy from the baroclinic conversion of zonal to eddy available potential energy." One inference from this result is that the stationary waves, and hence quasi-stationary behavior in the large scales, are maintained by baroclinic processes. This point is further advanced by RP, who argued that periods of quasi-stationary behavior in the large scales are integrally associated with an organized behavior of the synoptic scales.

The above-mentioned peculiar manner of energy transfer is a direct result of the absence of a momentum source (ψ^*) in the formulation adopted for the two-layer model. The absence of this source gives rise to the "Hadley circulation," a zonally symmetric, thermally driven, zonal flow in the upper layer, with *no flow in the lower layer.* The Hadley circulation is the only equilibrium solution in the absence of baroclinic instabilities. This purely zonal flow is the solution despite the presence of asymmetric topography in the lower layer. Forcing flow over the topography, e.g., in the form of ψ^*, alleviates some of the problems of the CS model. In particular, the basic state, which now necessarily contains lower layer flow and a topographically forced wave, is more realistic.

In their thermally driven two-layer models, Roads (1980a,b) and Yao (1980) force flow over the bottom surface by writing the surface vertical velocity in terms of the upper- and lower-layer mean streamfunctions. This removes the awkward situation of no flow in the lower layer by forcing flow over the topography. (Recall that in the CS and RP models the flow over the bottom surface is just the lower layer flow. If it is zero, then topography has little effect on the model response.) In the models of Roads (1980b) and Yao (1980) the purely zonal Hadley circulation is no longer a solution. Flow over topography necessarily gives rise to a zonally asymmetric state. Yao (1980) found that in certain parameter regimes the maintenance of the stationary waves was due mainly to the conversion of zonal to (stationary) eddy kinetic energy, while in others it was due mainly to the conversion of zonal to (stationary) eddy available potential energy. In either case the conversion of zonal kinetic to (stationary) eddy kinetic energy is *positive.* Although Yao's model is missing an important physical mechanism, ψ^*, he was able to obtain realistic energetics due to the bottom surface condition he imposed.

Several studies of "topographic" instability in the two-layer model of CS have challenged the claim that this instability is due to topography. In the model without topography, the instabilities are baroclinic. The results of a linear stability analysis show that all eigenvalues are complex, hence the name "propagating instabilities." In the presence of topography CS found the eigenvalues of the unstable waves to be purely real. These they named "stationary instabilities" or "orographic form-drag instabilities." Buzzi et al. (1984; hereafter referred to as BTS) analyzed a y-independent form of the CS model, concluding that two different types of topographic instability existed: one of an essentially baroclinic nature and the other of a mixed barotropic–baroclinic nature. The former is found in models with zonally symmetric basic states such as the CS model. The latter is present only in models with zonally asymmetric basic states, examples being the barotropic model of Charney and DeVore (1979) or a two-layer model with zonal momentum forcing (ψ^*). Yoden and Mukougawa (1983) and Mukougawa (1987) studied the energetics of "topographic instabilities" in the two-layer model. Their findings supported those of BTS. The energetics show that in the absence of a basic state with lower-layer flow, the topographic effect is such as to act as a sink for, not a source of, eddy kinetic energy. Thus this instability is actually baroclinic, not topographic, as its energy source is the available potential energy of the zonal flow. On the other hand, in the presence of an asymmetric basic

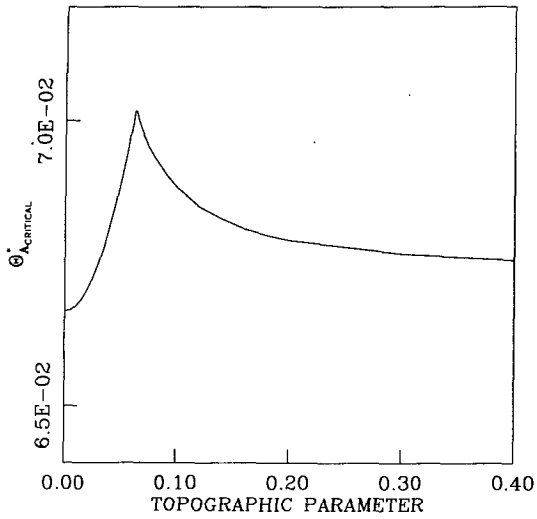

FIG. 17. The dependence of the stability of the Hadley equilibrium of the 1x-, 1y-system on topographic height.

state, the perturbation derives its energy mainly through the barotropic conversion of zonal kinetic to eddy kinetic energy. For this case the baroclinic energy conversion is negligible, and the instability is topographic.

In the absence of ψ^*, the Hadley circulation is the only equilibrium of the (1x, 1y) system for values of thermal driving θ_A^*, below the critical value for the onset of baroclinic instability. By drawing energy from the thermally driven Hadley solution, baroclinic instability induces flow in the lower layer, which then interacts with topography, giving rise to (a more properly termed) topographically modified baroclinic instability and wavy equilibria. Figure 17 shows the stability of the Hadley equilibrium as a function of topographic height. Topography actually stabilizes the flow by raising the value of the critical thermal driving, $\theta^*_{A\text{critical}}$, beyond which the flow becomes unstable. It is also noteworthy that for low topography, the first instabilities to appear as θ_A^* is increased beyond its critical value are propagating instabilities (i.e., traditional baroclinic). For higher θ_A^*, all instabilities are stationary (i.e., topographically modified baroclinic instabilities), while for still higher θ_A^*, all instabilities are once again propagating. For moderate and large values of topographic height, the first instabilities to appear are stationary, followed by the propagating type.

It is now not difficult to understand why in this type of thermally driven two-layer model the main process of energy conversion responsible for maintaining the wavy equilibria is baroclinic. The source of energy is the zonal available potential energy, which the topography cannot influence until the lower-layer flow is initiated through baroclinic instability. This situation changes when a momentum source is introduced into the model. Topographic disturbances directly forced by the lower level flow are then capable of converting zonal kinetic energy to eddy kinetic energy. This further diminishes the role played by the transient synoptic disturbances.

6. Weather regimes in the presence of momentum driving

The lateral flux of westerly momentum from the tropics is treated, in the present model, as a purely zonal barotropic forcing,

$$\psi^* = \psi_A^* \sqrt{2} \cos(y).$$

This forcing thus appears only in the equation for ψ_A,

$$\frac{\partial}{\partial t}\psi_A = k\psi_A^* + \text{other terms}.$$

Here k is a frictional coefficient taken to be the same as the Ekman friction parameter.

In Fig. 18 the behavior of the stable equilibrium point of the (1x, 1y) model is depicted for ψ_A^* ranging from 0.0 (no driving) to 0.10 (16 m s^{-1} driving). As before, this is a phase plot of the directly forced large-scale wave components, ψ_K versus ψ_L. Note that both the phase and the amplitude change as ψ_A^* is increased. The phase ranges from leading the trough of the topographic profile by 45° to lagging the trough by 45°. The amplitude of the response steadily increases with ψ_A^*. Figures 19a–d show a similar response of the 7x-, 7y-system attractor to the barotropic forcing. These are plots of the ψ_K versus ψ_L phase space trajectories for time steps 0 to 2000 (207 days). All runs were initialized at the same point. There are several noteworthy features. First of all, there is only one stable attractor. It took each run less than 35 days to reach their respective attractors. This is evidenced by the '□' marks, which denote periods of 10 days. The fact that the

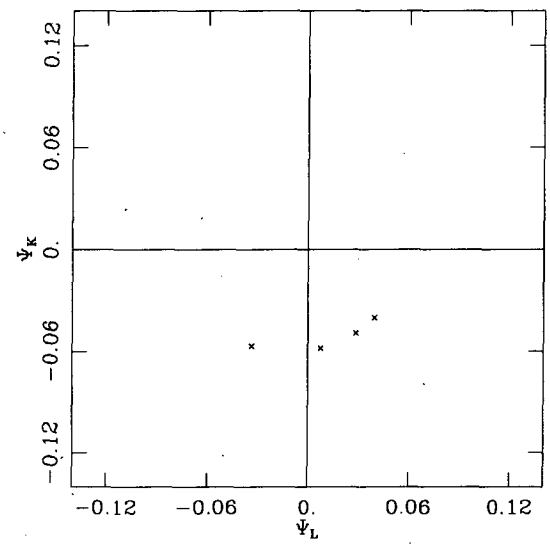

FIG. 18. Behavior of the stable equilibrium point of the 1x-, 1y-system as ψ_A^* is varied. From right to left: ψ_A^* = 0.0, 0.02, 0.05, 0.10.

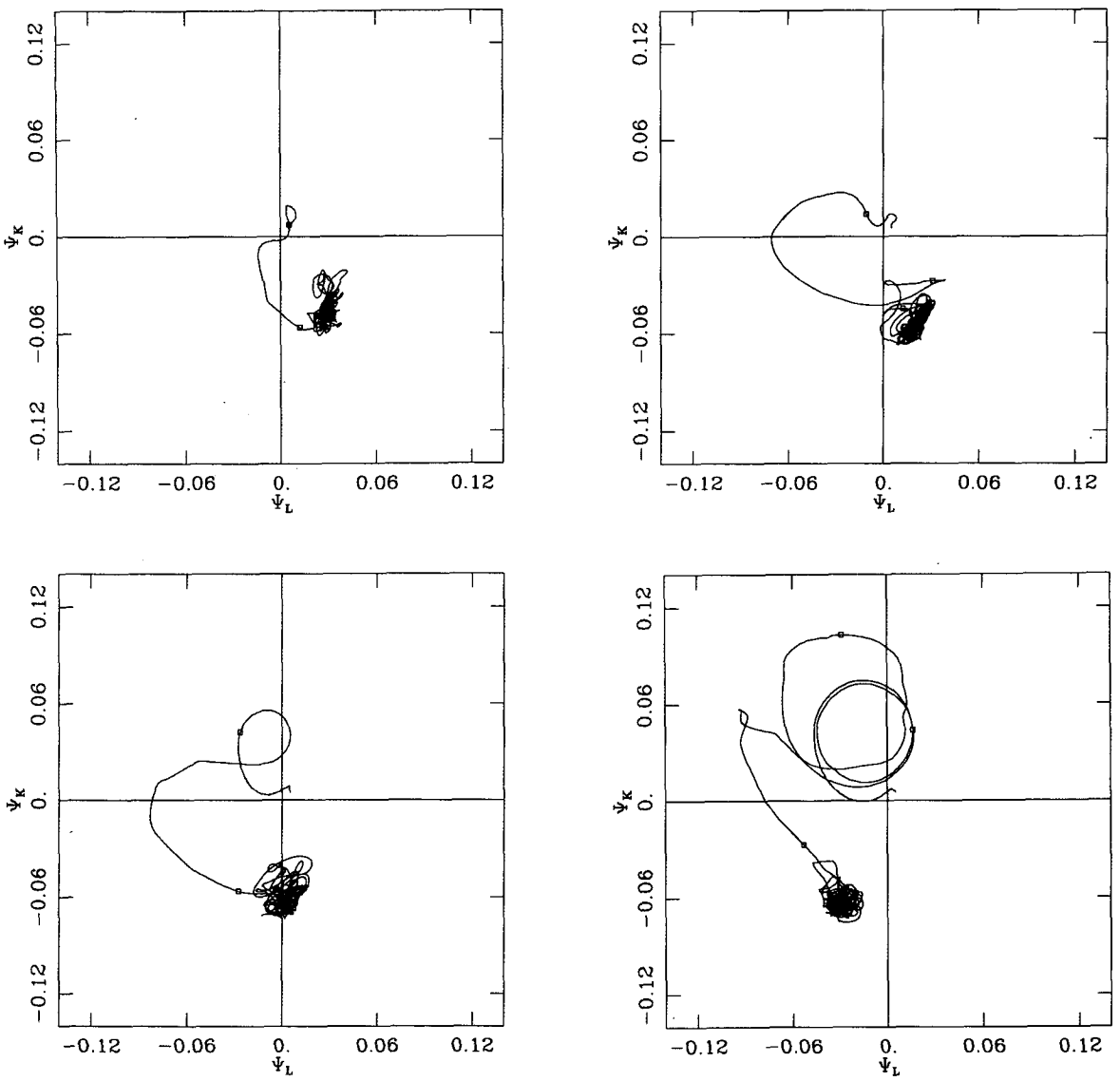

FIG. 19. Behavior of the ψ_K, ψ_L attractor of the 7x-, 7y-system as ψ_A^* is varied (all cases were initialized at the same random point and integrated for 2000 time steps). (a) $\psi_A^* = 0.0$, (b) $\psi_A^* = 0.02$, (c) $\psi_A^* = 0.05$, (d) $\psi_A^* = 0.10$. The squares mark periods of 10 days.

model quickly settles into the attractor underscores the importance of the single weather regime. Secondly, we see the same pattern of phase shift and increasing amplitude as with the (1x, 1y) model. These last features can be better grasped in Fig. 20. Figure 20 is a conglomeration of Figs. 19a–d, where 30-day running time means of time steps 500–2000 were calculated. As in Fig. 18, ψ_A^* increases from right to left. It is remarkable how consistently similar the stable equilibria of the (1x, 1y) model are to the attractors of the (7x, 7y) model.

It is apparent here that weather regimes in this model can be changed in response to changes in external forcing. This mechanism appears to be more viable than the organization of synoptic scales in bringing about a change. Not only the momentum driving, ψ_A^*, but also the thermal driving, θ_A^*, can alter the weather regime. Figures 21a and 21b are plots of ψ_K versus ψ_L for $\theta_A^* = 0.02$ (17 K), $\psi_A^* = 0.05$ (8 m s^{-1}) and $\theta_A^* = 0.05$ (27 K), $\psi_A^* = 0.05$ (8 m s^{-1}), respectively, for the (7x, 7y) model. Recall that without momentum driving ($\psi_A^* = 0$), only the purely zonal Hadley solution would exist at these values of θ_A^*. The presence of ψ_A^* forces flow over topography. This induces a wave, no matter how low θ_A^* is. In particular, at relatively low values of radiative forcing (e.g., 20 K– 30 K temperature difference across the channel) there is a wavy response manifested here by $\psi_K \neq 0$, $\psi_L \neq 0$. At this lower thermal driving, the high frequency components are less active. The

effect of drastically reducing the baroclinicity (from $\theta_A^* = 0.1$ to $\theta_A^* = 0.05$, and 0.02) is clear. The high-frequency components have a lot less energy. This translates to less variability in the low-frequency response.

7. Conclusion

It is not the intent of the present work to prove that multiple equilibria or multiple weather regimes do not exist. Rather, we studied the effects of full nonlinearity on the time-dependent response of the two-layer model for a given set of parameters. Under these circumstances only one weather regime was found.

By incorporating the destabilizing effect of the synoptic-scale waves but not the dissipative effect of the same waves, intermediate truncation levels tend to yield solutions drastically different from the fully nonlinear solutions. It was demonstrated that lower order models may exhibit "spurious chaos." These models do not have the proper channels through which energy can cascade upscale and vorticity can cascade downscale. The result is a highly chaotic solution that has little to do with the fully nonlinear, converged solution. Much of the chaos disappears when a sufficient number of modes are kept in the spectral expansion of the model variables. The conclusion, based on intermediate truncations, that the transient synoptic-scale waves are of primary importance not only in affecting weather at the synoptic scales, but also in inducing significant variability in the large scales, is not supported by the solution of the original governing partial differential equations. Although some high-frequency variability is inevitably induced by the synoptic scales through wave–wave interaction, the degree to which the low-frequency variability of the large scales is governed by the high frequency variability of the synoptic scales is put into question by the present study.

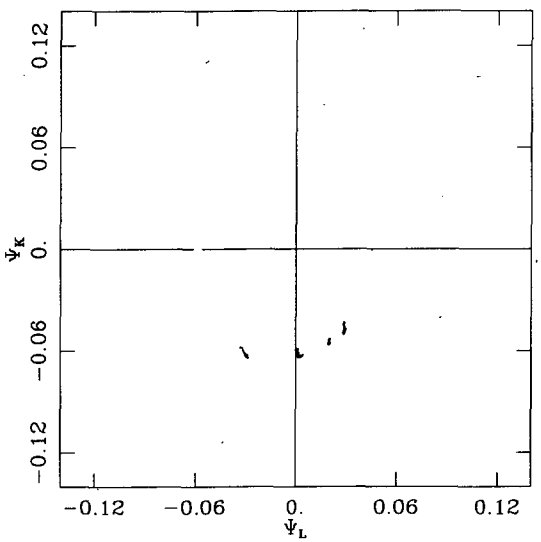

FIG. 20. 30-day running time mean of Figs. 17a–d from right to left: $\theta_A^* = 0.0, 0.02, 0.05, 0.10$. (Time steps 500–2000.)

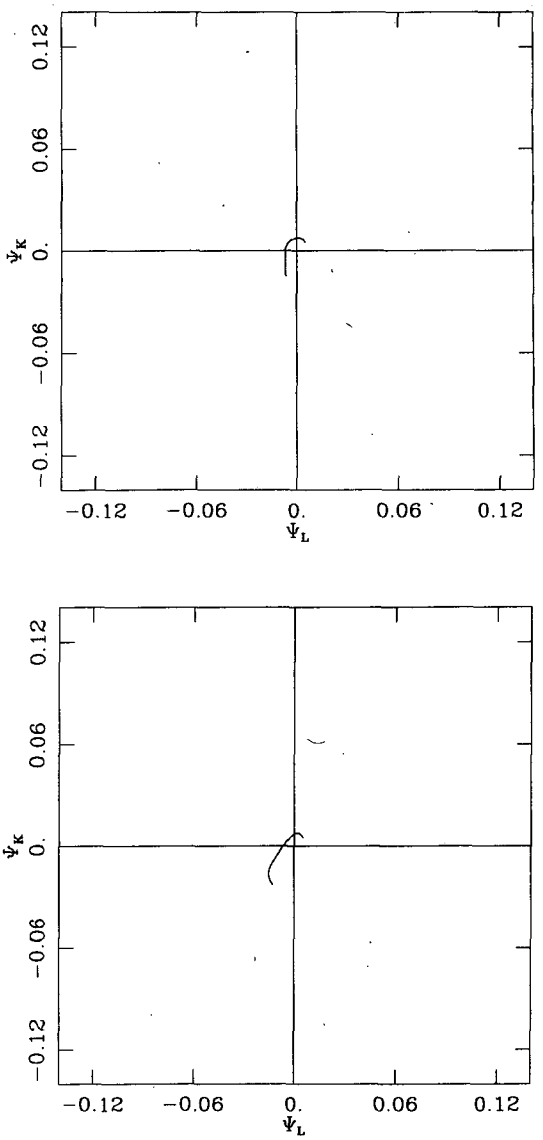

FIG. 21. As in Fig. 20 except that ψ_A^* is fixed at 0.05 and θ_A^* is varied. (a) $\theta_A^* = 0.02$, (b) $\theta_A^* = 0.05$.

It is remarkable how similar the large-scale wave components of our solution are to those of the $1x$-, $1y$-system, which excludes all effects of the small-scale, transient waves. The large-scale response of the fully nonlinear model follows the branch 1 solution curve of the $(1x, 1y)$ model as a function of thermal forcing. This was linked to an equilibration mechanism and to the dominance of the largest-scale waves for large values of the forcing.

We further noted a peculiarity in the formulation of most existing two-layer models that tends to exaggerate the role of baroclinic processes. This problem is alle-

viated by incorporating a barotropic, momentum forcing, ψ_A^*, into the model. Without this forcing the energetics of the model are somewhat awkward: the conversion of zonal kinetic energy to eddy kinetic energy is negative and the energy source for the stationary waves is solely the available potential energy of the flow.

The parameter values chosen for this study were those of RP's demonstration case. This was done in order to facilitate comparisons with the work of RP. However, with these parameters, the model atmosphere is probably unrealistically damped [viz., $k = 0.05$ (1 day Ekman damping time), $k' = 0.01$ (10 day damping time at the interface), $h'' = 0.045$ (2.2 day Newtonian cooling time).] Therefore, based on this study, we refrain from drawing conclusions regarding the earth's atmosphere. Reinhold and Pierrehumbert chose this set of parameters in order to obtain an earthlike response. Longer damping times resulted in absurd easterly flows in the lower layer of their model. In a fully nonlinear model with momentum forcing, this is no longer a problem. In Part III, we investigate the model response under more realistic parameter regimes.

Acknowledgments. The authors wish to thank R. T. Pierrehumbert, D. M. Straus and an anonymous reviewer for their helpful comments. The research is supported by National Science Foundation, Atmospheric Sciences Division, under grants ATM-8217616 and ATM-8606268. PC also received financial support from National Aeronautic and Space Administration under Grant NAGW 798, during her graduate studies at M.I.T. KKT further acknowledges the support from a Guggenheim Foundation fellowship during his sabbatical year.

APPENDIX A

Formulas for Computing the Interaction Coefficients and the β-term Coefficients

As described in section 2, the eigenfunctions, F_i, of the spectral expansion fall into three categories:

1) $f_{A(P_i)} = \sqrt{2}\cos(P_i y)$
2) $f_{K(M_i,P_i)} = 2\cos(M_i x)\sin(P_i y)$
3) $f_{L(H_i,P_i)} = 2\sin(H_i x)\sin(P_i y)$

where $P_i = 1, 2, \cdots$ and $M_i, H_i = 1, 2, \cdots$. In this context we supply general formulas for the interaction and β-term coefficients.

1. Interaction coefficients and their general formulas

The formal definition of the interaction coefficients is $c_{ijk} = \overline{F_i J(F_j, F_k)}$, where the overbar denotes a horizontal average. This algebraically tedious formula, which equals zero for most combinations of eigenfunctions, can be greatly simplified. The simple formulas are presented below. Only three combinations of eigenfunctions may yield non-zero interaction coefficients.

(i) $f_{A(P_i)}$, $f_{K(M_j,P_j)}$ and $f_{L(H_k,P_k)}$ determine the coefficient

$$C_{A(P_i)K(M_j,P_j)L(H_k,P_k)} = \frac{-2\sqrt{2}}{\pi} M_j \left\{ \frac{B1^2}{B1^2-1} - \frac{B2^2}{B2^2-1} \right\} \times \delta(M_j - H_k)\lambda(P_i + P_j + P_k)$$

where

$$B1 \equiv \frac{P_k + P_j}{P_i}, \quad B2 \equiv \frac{P_k - P_j}{P_i},$$

$$\delta(r) = 1 \quad \text{if} \quad r = 0$$
$$= 0 \quad \text{otherwise, and}$$
$$\lambda(r) = 1 \quad \text{if} \quad r \text{ is odd}$$
$$= 0 \quad \text{otherwise.}$$

(ii) $f_{K(M_i,P_i)}$, $f_{K(M_j,P_j)}$ and $f_{L(H_k,P_k)}$ determine the coefficient

$$\begin{aligned} C_{K(M_i,P_i)K(M_j,P_j)L(H_k,P_k)} = {} & S1\{\delta(M_i - H_k - M_j) \\ & \times \delta(P_i - P_k + P_j) - \delta(M_i - H_k - M_j)\delta(P_i + P_k - P_j) \\ & + [\delta(H_k - M_j + M_i) + \delta(H_k - M_j - M_i)] \\ & \times \delta(P_k + P_j - P_i)\} + S2\{\delta(M_i - H_k - M_j) \\ & \times \delta(P_i - P_k - P_j) + [\delta(H_k - M_j - M_i) \\ & + \delta(M_i + H_k - M_j)][\delta(P_i - P_k + P_j) \\ & - \delta(P_k - P_j + P_i)]\} \end{aligned}$$

where $S1 \equiv -(P_k M_j + P_j H_k)/2$ and $S2 \equiv (P_k M_j - P_j H_k)/2$.

(iii) $f_{L(H_i,P_i)}$, $f_{L(H_j,P_j)}$ and $f_{L(H_k,P_k)}$ determine the coefficient

$$\begin{aligned} C_{L(H_i,P_i)L(H_j,P_j)L(H_k,P_k)} = {} & S3\{[\delta(H_k - H_j - H_i) \\ & - \delta(H_k - H_j + H_i)]\delta(P_k + P_j - P_i) + \delta(H_k + H_j - H_i) \\ & \times \delta(P_k - P_j + P_i) - \delta(H_k + H_j - H_i)\delta(P_k - P_j - P_i)\} \\ & + S4\{\delta(H_k + H_j - H_i)\delta(P_k - P_j - P_i) + [\delta(H_k - H_j + H_i) \\ & - \delta(H_k - H_j - H_i)][\delta(P_k - P_j - P_i) \\ & - \delta(P_k - P_j + P_i)] \end{aligned}$$

where $S3 \equiv (P_k H_j + P_j H_k)/2$ and $S4 \equiv (P_k H_j - P_j H_k)/2$.

The above formulas generate interaction coefficients unique to within the possible permutations. (Recall that, in the old notation, $c_{ijk} = -c_{jik} = c_{kij} = c_{jki}$.) For example, consider the only nonzero interaction coefficient in the $1x$-, $1y$-mode model. It is a case (i) coefficient:

$$C_{A(1)K(1,1)L(1,1)} = C_{K(1,1)L(1,1)A(1)} = C_{L(1,1)A(1)K(1,1)}$$
$$= -C_{A(1)L(1,1)K(1,1)} = -C_{K(1,1)A(1)L(1,1)}$$
$$= -C_{L(1,1)K(1,1)A(1)} = -8\sqrt{2}/(3\pi).$$

2. β-term coefficients

The β-term coefficients are defined by

$$b_{ij} = \overline{F_i \partial F_j / \partial x}.$$

Although this formula is not as tedious as the definition of the interaction coefficients, it can be reduced to a trivial form. There is only one combination of eigenfunctions that results in nonzero b_{ij}:

(i) $F_{K(M_i,P_i)}$ and $F_{L(H_j,P_j)}$ determine the coefficient

$$b_{K(M_i,P_i)L(H_j,P_j)} = M_i \delta(M_i - H_j)\delta(P_i - P_j).$$

This relation, together with the fact that $b_{ij} = -b_{ji}$, determines all nonzero β-term coefficients. For example, the only nonzero β-term coefficient in the $1x$-, $1y$-system is

$$b_{K(1,1)L(1,1)} = -b_{L(1,1)K(1,1)} = 1.$$

APPENDIX B

Numerics

1. Time integration

The spectrally decomposed model equations form a nonlinear system of first-order ordinary differential equations in time. The equations were programmed in double precision and two packaged integration routines, ODE by Shampine and Gordon (1975) and D02BDG of the NAG Library, were tested against each other. Both codes determined that the equations were not numerically stiff. The time-dependent calculations in the present work were run using Shampine and Gordon's ODE code.

Data was recorded at intervals of 2.5 hours (or 1.0 in nondimensional time). Both ODE and the NAG routine use implicit methods, internally decreasing the integration step size until the desired accuracy is reached. We used a local relative and absolute error tolerance of 10^{-10}. Separate tests were run using the explicit Lorenz 4-cycle scheme. That routine was found to be inaccurate.

2. Bifurcation diagrams

The bifurcation diagrams of the $1x$-, $1y$-mode, six-equation system were generated by the continuation code of Rheinboldt and Burkardt (1983a,b). This code uses the pseudo-arc length method to trace bifurcation branches.

3. Stability of the large-scale equilibria

The stability of the large-scale [i.e., ($1x$, $1y$) model] equilibria to perturbations in the first x- and y-modes was determined by performing in a linearized stability analysis. The eigenvalues of this matrix were calculated using the NAG Library.

REFERENCES

Buzzi, A., A. Trevisan and A. Speranza, 1984: Instabilities of a baroclinic flow related to topographic forcing. *J. Atmos. Sci.*, **41**, 637–650.

Charney, J. G., and J. G. DeVore, 1979: Multiple flow equilibria in the atmosphere and blocking. *J. Atmos. Sci.*, **36**, 1205–1216.

——, and D. M. Straus, 1980: Form-drag instability, multiple equilibria and propagating planetary waves in baroclinic, orographically forced, planetary wave systems. *J. Atmos. Sci.*, **37**, 1157–1176.

——, J. Shukla and K. C. Mo, 1981: Comparison of a barotropic blocking theory with observation. *J. Atmos. Sci.*, **30**, 762–779.

Curry, J. H., J. R. Herring, J. Loncaric and S. A. Orszag, 1984: Order and disorder in two- and three-dimensional Bénard convection. *J. Fluid Mech.*, **147**, 1–38.

Davey, M. K., 1980: A quasi-linear theory for rotating flow over topography. Part 1. Steady β-plane channel. *J. Fluid Mech.*, **99**, 267–292.

——, 1981: A quasi-linear theory for rotating flow over topography. Part 2. Beta-Plane annulus. *J. Fluid Mech.*, **103**, 297–320.

Källén, E., 1983: A note on orographically induced instabilities in two layer models. *J. Atmos. Sci.*, **40**, 500–505.

Klein, P., and J. Pedlosky, 1986: A numerical study of baroclinic instability at large supercriticality. *J. Atmos. Sci.*, **43**, 1243–1262.

Lorenz, E. N., 1960: Energy and numerical weather prediction. *Tellus*, **12**, 364–373.

——, 1963: The mechanics of vacillation. *J. Atmos. Sci.*, **20**, 448–464.

——, 1971: An *N*-cycle time-differencing scheme for stepwise numerical integration. *Mon. Wea. Rev.*, **99**, 644–648.

Marcus, P. S., 1981: Effects of truncation in modal representations of thermal convection. *J. Fluid Mech.*, **103**, 241–255.

Mukougawa, H., 1987: Instability of topographically forced Rossby waves in a two-layer model. *J. Meteor. Soc. Japan* (in press).

Orszag, S. A., and L. C. Kells, 1980: Transition to turbulence in plane Poiseuille and plane Couette flow. *J. Fluid Mech.*, **96**, 159–205.

Rambaldi, S., 1982: Multiple equilibria and their stability in a barotropic and baroclinic atmosphere. Ph.D. thesis, M.I.T.

——, and K. C. Mo, 1984: Forced stationary solutions in a barotropic channel: Multiple equilibria and theory of nonlinear resonance. *J. Atmos. Sci.*, **A1**, 3135–3146.

Reinhold, B. B., 1981: Dynamics of weather regimes: Quasi-stationary waves and blocking. Ph.D. thesis, M.I.T.

——, and R. T. Pierrehumbert, 1982: Dynamics of weather regimes: Quasi-stationary waves and blocking. *Mon. Wea. Rev.*, **110**, 1105–1145.

——, and ——, 1985: Corrections to "Dynamics of weather regimes: Quasi-stationary waves and blocking." *Mon. Wea. Rev.*, **113**, 2055–2056.

Rheinboldt, W. C., and J. V. Burkardt, 1983a: A locally parameterized continuation process. *A.C.M. Trans. Math. Software*, **9**, 215–235.

——, and ——, 1983b: Algorithm 596: A program for a locally parameterized continuation process. *A.C.M. Trans. Math. Software*, **9**, 236–241.

Roads, J. O., 1980a: Stable near-resonant states forced by perturbation heating in a simple baroclinic model. *J. Atmos. Sci.*, **37**, 1958–1967.

——, 1980b: Stable near-resonant states forced by orography in a simple baroclinic model. *J. Atmos. Sci.*, **37**, 2381–2395.

——, 1982: Stable and unstable near-resonant states in multilevel severely truncated, quasi-geostrophic models. *J. Atmos. Sci.*, **39**, 203–224.

Salmon, R., 1978: Two-layer quasi-geostrophic turbulence in a simple special case. *Geophys. Astrophys. Fluid Dyn.*, **10**, 25–53.

——, 1980: Baroclinic instability and geostrophic turbulence. *Geophys. Astrophy. Fluid Dyn.*, **15**, 167–211.

Shampine, L. F., and M. K. Gordon, 1975: *Computer Solution of Ordinary Differential Equations: The Initial Value Problem.* Freeman.

Stone, P. H., 1978: Baroclinic adjustment. *J. Atmos. Sci.*, **35**, 561–571.

Tung, K. K., and A. J. Rosenthal, 1985: Theories of multiple equilibria—A critical reexamination. Part I: Barotropic models. *J. Atmos. Sci.*, **42**, 2804–2819.

——, and ——, 1986: On the extended-range predictability of large-scale quasi-stationary patterns in the atmosphere. *Tellus*, **38A**.

Yao, M.-S., 1980: Maintenance of quasi-stationary waves in a two-level quasi-geostrophic spectral model with topography. *J. Atmos. Sci.*, **37**, 29–43.

Yoden, S., 1983a: Nonlinear interactions in a two-layer, quasi-geostrophic, low-order model with topography. Part I: Zonal flow-forced wave interactions. *J. Meteor. Soc. Japan*, **61**, 1–18.

——, 1983b: Nonlinear interactions in a two-layer, quasi-geostrophic, low-order model with topography. Part II: Interactions between zonal flow, forced waves and free waves. *J. Meteor. Soc. Japan*, **61**, 19–35.

——, and H. Mukougawa, 1983: Instabilities of a baroclinic zonal flow in the presence of surface topography. *J. Meteor. Soc. Japan*, **61**, 789–804.